Chemical Geology 637 (2023) 121674

Contents lists available at ScienceDirect

Chemical Geology

journal homepage: www.elsevier.com/locate/chemgeo

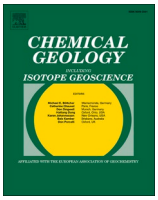

Impact of wet-dry cycles on enhanced rock weathering of brucite, wollastonite, serpentinite and kimberlite: Implications for carbon verification

Amanda R. Stubbs [a,b,*], Ian M. Power [a], Carlos Paulo [a,c], Baolin Wang [d], Nina Zeyen [d,e], Sasha Wilson [d], Evelyn Mervine [f,g], Chris Gunning [h]

[a] Trent School of the Environment, Trent University, Peterborough, ON K9L 0G2, Canada
[b] School of Geographical and Earth Sciences, University of Glasgow, Glasgow G12 8QQ, United Kingdom
[c] SRK Consulting (Canada) Inc, Toronto, ON M5H 3B7, Canada
[d] Department of Earth and Atmospheric Sciences, University of Alberta, Edmonton, AB T6G 2E3, Canada
[e] Department of Earth Sciences, University of Geneva, Rue des Maraîchers 13, 1205 Geneva, Switzerland
[f] Group Technical & Sustainability, Anglo American, 201 Charlotte Street, Brisbane, QLD, 4000, Australia
[g] School of the Environment, The University of Queensland, St. Lucia, QLD, 4072, Australia
[h] SGS Canada Inc., Lakefield, Ontario K0L 2H0, Canada

ARTICLE INFO

Editor: Oleg Pokrovsky

Keywords:
Enhanced rock weathering
CO_2 mineralization
CO_2 sequestration
Kimberlite
Brucite
Wollastonite skarn
Stable isotopes
Radiocarbon dating
Carbon verification

ABSTRACT

Enhanced rock weathering is a proposed CO_2 removal strategy for mitigating climate change; its implementation can be facilitated by improving carbon verification methods. In this study, weathering experiments exposed brucite, wollastonite skarn, serpentinite, and kimberlite residues (Venetia Diamond Mine, South Africa), to wetting and drying cycles (4/day) for 1 yr to elucidate reaction pathways and rates while evaluating carbon verification tools, including mineral quantification, total inorganic carbon (TIC), and stable and radiogenic carbon isotopes. Two primary reaction pathways were identified: A) silicate and hydroxide dissolution leading to carbonate precipitation (desirable), and B) dissolution and reprecipitation of carbonates (undesirable). The kimberlite residues, containing serpentine (19–33 wt%) and calcite (4–5 wt%), experienced variable and minor changes in total inorganic carbon. The $\delta^{13}C$ and $\delta^{18}O$ values of the carbonate minerals approached those expected for atmospheric-derived CO_2 and are best explained by the exchange of carbonate CO_2 with atmospheric CO_2 (pathway A) as opposed to net CO_2 sequestration. In contrast, the reaction of brucite (1.22% to 5.98%) and wollastonite skarn (0.22% to 1.01%) with atmospheric CO_2 was substantial, as indicated by the increases in TIC (pathway B) yet decreases in $\delta^{13}C$ values were inconsistent with the incorporation of atmospheric CO_2 as a result of kinetic isotope fractionation due to carbonation being CO_2 supply limited. The pulverized serpentinite experience insufficient carbonation to be detected by TIC. Unweathered (blue ground) and naturally weathered (yellow ground) kimberlite from the Voorspoed Diamond Mine, South Africa were compared to kimberlite residues used in experiments. Yellow ground contained twice the TIC content compared to blue ground whereas quantitative scanning electron microscopy revealed calcite veinlets that are characteristic of secondary mineralization. While the blue and yellow ground samples were essentially radiocarbon dead (0.03 and 0.05 $F^{14}C$, respectively), substantial modern carbon was incorporated into the kimberlite (up to +0.27 $F^{14}C$; CO_2 exchange), brucite (+0.55 $F^{14}C$), and wollastonite skarn (+0.53 $F^{14}C$; CO_2 sequestration) powders during weathering experiments. Although stable and radiogenic carbon isotopes have been used to verify the mineralization of atmospheric CO_2, these methods are affected by CO_2 exchange and kinetic fractionation effects during weathering that can be misleading and, thus, should not be relied on as sole methods for carbon verification.

* Corresponding author at: Trent School of the Environment, Trent University, Peterborough, ON K9L 0G2, Canada.
E-mail address: amandastubbs@trentu.ca (A.R. Stubbs).

https://doi.org/10.1016/j.chemgeo.2023.121674
Received 28 July 2023; Accepted 9 August 2023
Available online 12 August 2023

1. Introduction

The development and implementation of negative emission technologies (NETs) has been advised by the United Nations Framework Convention on Climate Change to meet global reduction targets (EASAC, 2018). Low cost and energy NETs such as enhanced rock weathering (ERW) aim to store carbon as either an aqueous (e.g., HCO_3^-) or solid (e.g., carbonate mineral) phase (Andrews and Taylor, 2019; Beerling et al., 2018; Taylor et al., 2015; Wilson et al., 2011; Wilson et al., 2014). ERW involves dispersing pulverized alkaline rocks over large areas where these materials weather and react with atmospheric CO_2 (Renforth, 2012). Similarly, passive CO_2 mineralization of fine-grained ultramafic and mafic mine wastes can occur via weathering within impoundments at mine sites. In both processes, CO_2 sequestration occurs where fine-grain alkaline materials with high surface areas are exposed to weathering, including dissolution of silicate and hydroxide minerals and precipitation of secondary carbonates during wetting and drying periods (Stubbs et al., 2022; Wilson et al., 2014). Rock and mineral feedstocks including powdered brucite [$Mg(OH)_2$], wollastonite skarn ($CaSiO_3$) skarn, and serpentine group minerals [$Mg_3Si_2O_5(OH)_4$] in serpentinite have been studied for ERW and are used in this study due to their desirable mineralogy and varying degrees of reactivity. In addition to these powered rocks, kimberlite residues from the Venetia Diamond Mine in South Africa were used as a feedstock for CO_2 mineralization.

This study is part of De Beers' Project CarbonVault, a research program designed to capture and store carbon via mineral carbonation of kimberlite from diamond mines. Prior to this project commencing, only a few studies had explored CO_2 mineralization at diamond mines (Rollo and Jamieson, 2006; Wilson et al., 2011; Wilson et al., 2009b); however, recent studies have further examined the potential of kimberlite mine wastes to sequester CO_2, including reactivity with CO_2 and direct measurement of CO_2 drawdown in these wastes (Mervine et al., 2018; Paulo et al., 2021; Stubbs et al., 2022). Kimberlite residues are a desirable feedstock for ERW as this would make use of a waste product that requires no additional comminution (Li et al., 2018), and they have favorable mineralogical and geochemical compositions (Stubbs et al., 2022). These residues from the Venetia Diamond Mine, South Africa, have the capacity to draw down CO_2 during rainfall simulation as demonstrated by Stubbs et al. (2022) and are a desirable feedstock for ERW (Paulo et al., 2021).

Water plays a vital role in carbonation reactions as it is needed to promote cation release, hydration of CO_2, and carbonate mineral precipitation (Power et al., 2013b), a crucial part of the inorganic carbon cycle. In nature, wetting and drying cycles depend on precipitation events (i.e., rainfall; Yang et al., 2009). The release of cations, including Mg^{2+} and Ca^{2+}, occurs during the dissolution of minerals and, once released into solution, they are available for carbonate precipitation (Power et al., 2013b). At mines, tailings and other waste products are exposed to wetting periods through precipitation events including rainfall or exposure to process waters (Fall et al., 2009; Stubbs et al., 2022). After residues have been exposed to a wetting period, they may dry, allowing evaporation to drive precipitation of secondary carbonate minerals (Acero et al., 2007; Acero et al., 2009; Bea et al., 2012; Wilson et al., 2011; Wilson et al., 2014). Experiments in this study were designed to simulate natural wetting and drying to initiate carbonation of the respective feedstocks.

Carbon verification is necessary to ensure the reliability and credibility of carbon removal (IPCC, 2022). Identifying sources and sinks of carbon to understand how carbon is cycled in complex open systems, such as mine sites, remains challenging. For instance, carbonate minerals that form from the weathering of kimberlite mine wastes at diamond mines may incorporate a range of carbon sources including mantle carbon from the kimberlite, sedimentary carbon from country rock, carbonate formed though kimberlite alteration, modern or ancient organics (e.g., degraded vegetation or even bitumen), and atmospheric CO_2 (Wilson et al., 2011). Carbon can often be recycled through rock weathering, making it challenging to determine if atmospheric CO_2 has been sequestered. Stable carbon and oxygen isotopes of secondary carbonates have been used to identify carbon sources and sinks to demonstrate the sequestration of atmospheric CO_2 (Flude et al., 2017; Oskierski et al., 2013; Wilson et al., 2011). Additionally, radiocarbon can be used as a tracer for atmospheric CO_2 (Finstad et al., 2023) as it can determine whether or not modern carbon has been incorporated into carbonate minerals and can provide a quantitative estimate for the sequestration of modern carbon (Oskierski et al., 2013; Wilson et al., 2011). In this study, a variety of tools including total inorganic carbon, mineralogy, and stable and radiogenic carbon isotopes were used to understand carbon cycling in simulated weathering experiments with few carbon sources.

This study investigated weathering of kimberlite residues and rock powder for CO_2 removal with the goals of (1) better understanding the effects of wetting and drying cycles on weathering, (2) determining CO_2 removal rates, (3) elucidating carbon cycling using stable and radiogenic carbon isotopes, (4) characterizing yellow ground (i.e., weathered kimberlite) in the context of CO_2 mineralization, and (5) scrutinizing carbon verification techniques. To accomplish these goals, year-long wet-dry cycling experiments were performed using rock powders (brucite, wollastonite skarn, and serpentinite) and kimberlite residues from the Venetia Diamond Mine in South Africa. These results are compared to blue ground (i.e., unweathered kimberlite) and rare yellow ground samples that formed through prolonged weathering of kimberlite. The findings from this study have implications for the use of kimberlite residues for enhanced weathering and highlight the importance of using multiple carbon verification techniques to monitor CO_2 sequestration.

2. Methods

2.1. Fieldwork and sampling

Fieldwork and sampling were conducted at the Venetia Diamond Mine, South Africa (Fig. 1A, C, and E), in May 2017 and 2018 at the fine residues deposits (FRDs) and ore stockpiles. The fine residues are highly heterogeneous due to the complex mineralogy of the kimberlite pipes, incorporation of variable amounts and types of country rock during mining, and the mixing of kimberlite facies during processing. Kimberlite residues at Venetia are not routinely sampled and analyzed, and therefore, there is little information regarding their composition. Residue samples used in this study were also used in previous studies measuring CO_2 fluxes (Stubbs et al., 2022) and cation release (Paulo et al., 2021). Several kilograms of dark volcanoclastic kimberlite (DVK) were collected from the ore stockpile, placed in plastic bags, and further processed in the laboratory. A bulk sample (several kilograms) of fine residues was collected in large buckets as a slurry from one of the outlet pipes at the FRD where some of the fines were lost when excess water was discarded. Additional samples were collected at depth from the FRD using a soil corer and at one location with the aid of a backhoe that created a vertical face.

Sampling was also conducted at the Voorspoed Diamond Mine, South Africa (Fig. 1B, D and F). Three field campaigns were conducted in 2016, 2017, and 2018 to collect weathered kimberlite samples. Two types of blue ground were sampled including unweathered rock and freshly pulverized kimberlite residues. Yellow ground, intermediately weathered kimberlite, and thin carbonate coatings on cobbles of weathered kimberlite were collected from the pre-1912 impoundment where kimberlite rock and residues had been exposed to >100 years of weathering. Multiple samples were 10s of centimetres in size and were collected from the surface of the pre-1912 impoundment in plastic bags.

Wollastonite skarn samples (20.1 wt% pure) were provided as soil amendment packages of sand-sized material from the Canadian Wollastonite skarn quarry near Kingston, Ontario, Canada. Brucite (73.5 wt% pure) was sourced from the Brucite Mine, Nevada, United States and the serpentinite (95.7 wt% pure) was sourced from the Lizard

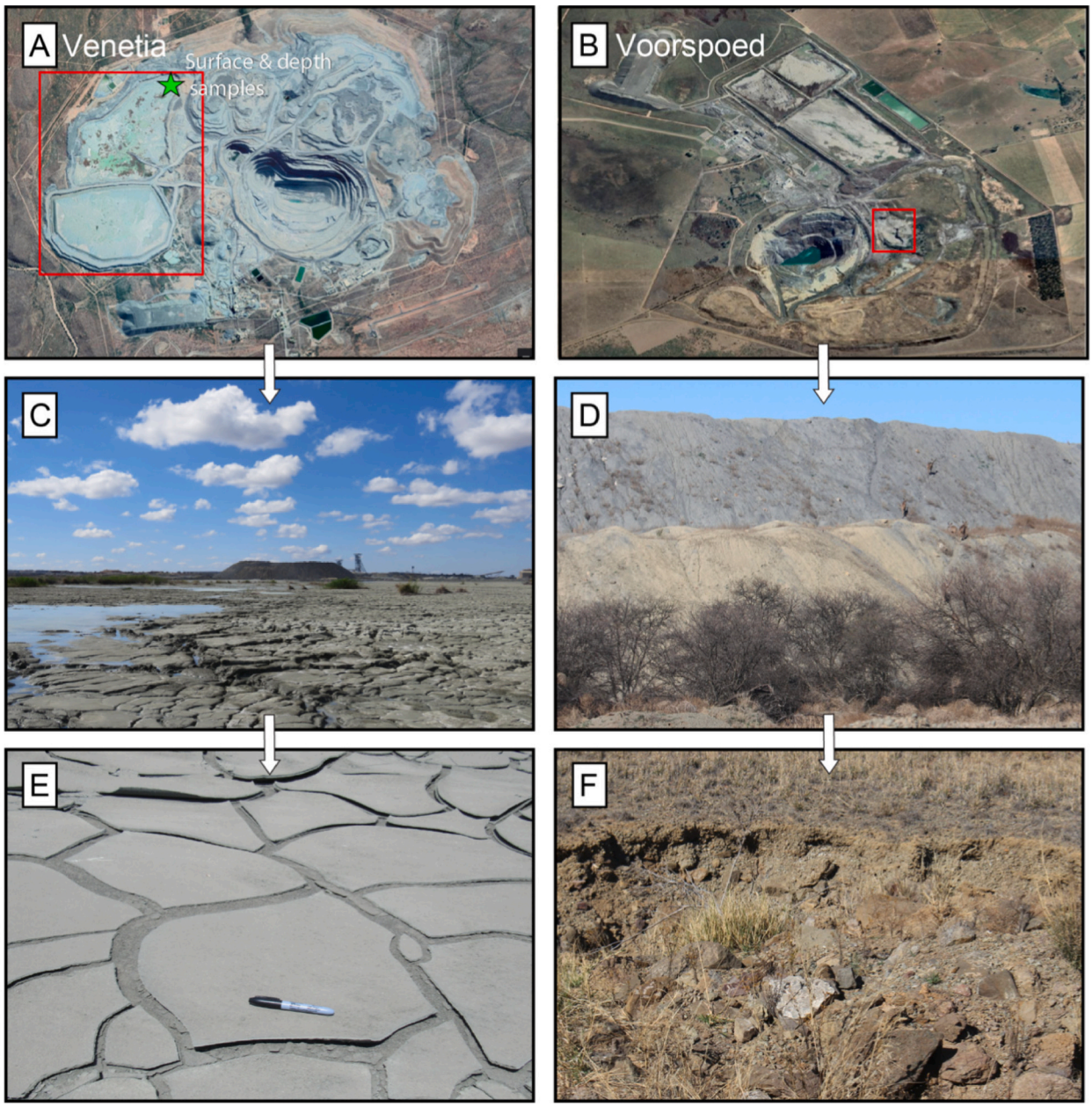

Fig. 1. Photographs of the Venetia and Voorspoed diamond mines in South Africa. A: Satellite image of the Venetia mine, highlighting the Fine Residues Deposits (FRDs; red box) and sampling area (green star). B: Satellite image of the Voorspoed mine with the pre-1912 mine wastes outlined by red box. C: Photograph of the Venetia FRD, illustrating the variable water conditions that may exist, including ponding (left) and desiccation (right). D: Photograph of the Voorspoed pre-1912 impoundment showing partial natural revegetation. E: Photograph of the Venetia fine residues showing desiccation cracks (marker for scale). F: Closer view of the historic Voorspoed mine wastes from which the yellow ground sample was collected. (For interpretation of the references to colour in this figure legend, the reader is referred to the web version of this article.)

Ophiolite, United Kingdom. Brucite and wollastonite skarn were chosen for this study as they have been extensively studied for CO_2 mineralization (Daval et al., 2009, 2010; Harrison et al., 2015; Harrison et al., 2013; Kojima et al., 1997; Power et al., 2021) and have relatively simple mineralogy and fast dissolution rates compared to the kimberlite residues. Serpentine minerals were selected as they are amongst the most abundant minerals in the Venetia kimberlite residues (Stubbs et al., 2022) and other ultramafic mine wastes (Power et al., 2013c; Pronost et al., 2012; Wilson et al., 2009a), making them important minerals to consider for mine waste carbonation.

2.2. *Wet-dry cycling experiments*

Wet-dry cycling experiments (Fig. 2) were conducted under laboratory conditions using fine kimberlite residues (17VEN-FRD1-P1K, 17VEN-FRD2-Cyclone-SampleB), pulverized DVK (K01 DVK2 and 2018 DVK) and rock powders containing wollastonite skarn, brucite and serpentine (Table 1). No modifications to the FRD residues were made for weathering experiments. Samples of Dark Volcanoclastic Kimberlite (DVK) ore were crushed using a sledgehammer to a grain size of <1.6 cm and then pulverized (FLSmidth Essa® LM2 Pulverizing Mill) for 5 s to a final particle size <1 mm. Brucite, wollastonite skarn, and serpentinite samples were pulverized for 15, 30, and 40 s until median particle diameters (D50) of 8, 52, and 100 μm were achieved, respectively. These

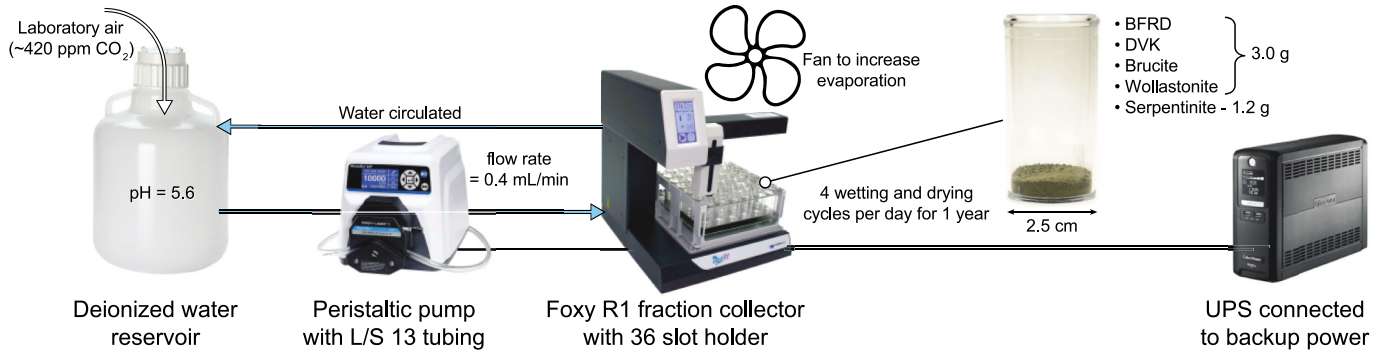

Fig. 2. Schematic of experimental apparatus for the wet-dry cycling experiments. Deionized water was continuously bubbled with laboratory air (~420 ppm CO_2) to maintain a pH of 5.6 and was delivered to the Foxy R1 fraction collector at a flow rate of 0.4 mL/min using a peristaltic pump. Samples were placed in the holder, exposing them to 4 wet-dry cycles per day using a fan to increase evaporation. The Foxy R1 and the peristaltic pump were plugged into an uninterrupted power supply that was connected to backup power to ensure the experiment was not interrupted.

Table 1
Sample list for wet-dry cycling experiments including localities, masses and number of vials.

Sample	Locality	Mass (g)	Number of vials
17VEN-FRD1-P1-K	Venetia - FRD1	3.0	20
17VEN-FRD2-Cyclone-SampleB	Venetia - FRD2	3.0	20
K01 DVK2	Venetia - stockpile	3.0	20
2018 DVK	Venetia - stockpile	3.0	20
Brucite	Nevada, USA	3.0	4
Wollastonite skarn	Kingston, Canada	3.0	20
Serpentinite	Lizard Ophiolite, UK	1.6	20

times were determined after testing different pulverizing intervals for each sample until the most representative grain size was achieved. All samples were homogenized prior to beginning the experiments.

Plastic 7-dram vials (=25 mL, diameter = 2.5 cm) were used to hold samples in a 36-slot sample rack. Aliquots (3.00 g) of Venetia residues sampled from the FRD were placed in each of the 36 slots in the first of two experiments: 17VEN-FRD1-P1K, 17VEN-FRD2-Cyclone-SampleB, K01 DVK2, and 2018 DVK. The second experiment used aliquots (3.00 g) of 2018 DVK, wollastonite skarn, and brucite, resulting in thicknesses of 0.2–0.5 cm. Smaller aliquots (1.60 g) were used for serpentinite samples due to slower infiltration and drying times relative to other samples. For each of the samples 20 different vials were used to allow for duplicate analysis, with the exception of brucite, which only utilized 4 vials due to limited sample slots.

Experiments utilized two Foxy R1 fraction collectors (36 sample position) from Teledyne ISCO and a Masterflex L/S Network-Compatible Pump System fitted with L/S® 13 tubing that drew deionized water (18.2 MΩ·cm) from two 20 L Nalgene carboys to the inlet ports on the Foxy R1 collectors. Masterflex® L/S® 14 tubing was connected to the waste port of the collectors to allow circulation of deionized water back to the reservoirs when not being dispensed to samples. Air was constantly bubbled through the reservoirs. The pH of the deionized water was measured using an Orion Star A321 pH meter and was consistently at 5.6, which indicates the water was at equilibrium with atmospheric CO_2. The peristaltic pump was set to a flow rate of 0.4 mL/min and the Foxy R1 was programmed to dispense water for 1 min (0.4 mL) to each of the 36 sample containers every 6 h. Prior to initiating experiments, it was determined that 0.4 mL of water was needed to wet, but not saturate, 3.0 g of sediment. The flow rate was checked every 3 months to ensure the proper amount of water continued to be dispensed. Equipment was plugged into an uninterrupted power supply (900 W capacity), which was connected to the building's backup power (Fig. 2).

A large fan (50 × 50 cm) was placed over each of the Foxy R1 collectors to reduce drying time and enable four wet-dry cycles per day (average of 122 per month), simulating more rainfall events. A YesAir air quality monitor from Critical Environment Technologies™ was used to track temperature, relative humidity, and CO_2 concentrations for the duration of the experiment. The temperature stayed consistent within 5 °C, the relative humidity stayed consistent within 10%, and the CO_2 concentration stayed within 15 ppm (398–413 ppm CO_2).

Sample vials were collected according to the following schedule: every 2 weeks (first month), once per month (1–6 months), and then at 8, 10 and 12 months. Experiments ran for a total of 1 yr and 2 weeks. Samples were replaced with new ones for duplicates in reverse order, e.g., replacing the 2-week sample would then become the 1-year sample later in the experiment. All samples were analyzed for total inorganic carbon (TIC) and 3-, 6- and 12-month samples were also analyzed for their stable carbon and oxygen isotope compositions. Initial and final samples for 17VEN-P1K, 2018 DVK, wollastonite skarn, and brucite were analyzed for radiocarbon. Secondary precipitates of the 12-month samples were imaged using a stereomicroscope and scanning electron microscope (SEM) and analyzed with energy dispersive spectroscopy (EDS) and X-ray diffraction (XRD) to assess their chemical and mineralogical compositions.

2.3. Blue and yellow ground samples

Blue ground and yellow ground rock samples were crushed into smaller fragments using a sledgehammer. Subsamples of these rocks were collected, pulverized, and homogenized for further geochemical, mineralogical, and isotopic analysis. Surficial, mm-scale carbonate coatings (n = 11) were collected from the remaining yellow ground samples using a metal dental scribe for stable carbon and oxygen isotope analysis.

Selected blue and yellow ground samples were embedded in epoxy. Two parts Buehler® epoxy mounting resin and one-part Buehler® hardener were mixed in a 15 mL centrifuge tube. Mixes were degassed in a desiccator for 2 min, poured into molds (25 mm diameter) containing the samples, degassed for an additional 2 min and left to cure at room temperature for a minimum of 9 h. These embedded samples were polished using a Buehler® EcoMet 30 polisher to a final finish using 0.05 μm polishing suspension and a TriDent polishing cloth. Samples were then analyzed using QEMSCAN to map their mineralogical compositions. In addition, polished thin sections (27 × 46 mm) of blue and yellow ground samples were made by Vancouver Petrographics Ltd., Canada.

2.4. Analytical methods

2.4.1. Geochemistry

Venetia, Voorspoed, and powdered rock samples were analyzed for total inorganic carbon (TIC) using a Model CM5017 Coulometer from UIC Inc. at Trent University. These methods are consistent with the TIC protocol by Stubbs et al. (2022). In addition, samples were analyzed for their bulk geochemical compositions using X-ray fluorescence (XRF) spectroscopy by SGS Canada Inc., Lakefield, Ontario, Canada. Compositions were reported as percent oxides with detection limits ranging from 0.0001 to 0.01% (Table S1). Detailed methods for TIC and XRF are available as Supplementary Material.

2.4.2. Mineralogy

X-ray diffraction (XRD) patterns on initial samples (Tables 2 and 3) were collected under 20–30% relative humidity (RH) using a Bruker D8 Advance θ–θ powder X-ray diffractometer equipped with a LYNXEYE XE-T 1D Position Sensitive Detector in the Environmental Economic Geology Laboratory, University of Alberta. Mineral phase identification was conducted using the DIFFRAC.EVA XRD phase analysis software (Bruker) with reference to the International Center for Diffraction Data Powder Diffraction File 4+ database (ICDD PDF4+). Rietveld refinements (Bish and Howard, 1988; Hill and Howard, 1987; Rietveld, 1969) with XRD data were used to determine mineral abundances with TOPAS 5 (Bruker). Major, minor, and trace minerals range from 10 to 100 wt%, 1–10 wt%, and < 1 wt%, respectively. Detailed methods are available as Supplementary Material.

The qualitative mineralogy of secondary precipitates that formed during wetting and drying experiments was determined using X-ray diffraction at SGS in Lakefield, Ontario, Canada. Each sample was hand ground using a mortar and pestle in anhydrous ethanol prior to being mounted as a slurry on a zero-diffraction quartz plate. XRD data were collected using a BRUKER AXS D8 Advance Diffractometer. Mineral phase identification was conducted using DIFFRAC.EVA XRD phase analysis software (Bruker) with reference to the International Center for Diffraction Data Powder Diffraction File 4+ database (ICDD PDF4+).

2.4.3. Microscopy

Secondary precipitates formed in the weathering experiments were sampled using tweezers and examined using SEM and EDS at The University of Western Ontario in the Nanofabrication Facility in London, Ontario, Canada following the same protocol by Stubbs et al. (2022). These detailed methods are available as Supplementary Material.

Embedded blue and yellow ground specimens were examined using Quantitative Evaluation of Materials by Scanning Electron Microscopy (QEMSCAN). The QEMSCAN system uses a Carl Zeiss Evo 50 scanning electron microscope (SEM) coupled with four dispersive X-ray spectrometers to image and mineralogically map samples. QEMSCAN utilizes both the back-scattered electron signal intensity as well as an Energy Dispersive X-ray Signal at each measurement point. The Field Scan (FS) Mode of measurement was utilized for these sections. The FS mode of measurement maps a core sample that has been mounted in the polished section and collects a chemical spectrum at a set interval within the field of view. Each field of view is then processed offline and a pseudo image of the core sample is produced.

Polished thin sections (27 × 46 mm) of the samples were made by Vancouver Petrographics Ltd. and examined under plane- and cross-polarized light using a Zeiss Axioscope 5 microscope equipped and images obtained using an Axiocam 208 colour camera.

2.4.4. Stable and radiogenic isotopes

A suite of Venetia kimberlite residues ($n = 14$) was analyzed for their stable carbon and oxygen isotopes by Jan Veizer Stable Isotope Laboratory in Ottawa, Canada. Four of these samples were used in wetting and drying experiments (Table 1). Samples were loaded into exetainers and 0.1 mL of H_3PO_4 (S.G. 1.91) was added to the interior wall of each exetainer. The exetainers were then capped and helium-flushed while horizontal to prevent reaction between the sample and H_3PO_4. Once flushed, samples containing calcite were reacted at 25 °C for 24 h and samples containing magnesite were reacted at 70 °C for 4 h. The measurements were performed on a Delta XP and a Gas Bench II, both from Thermo Finnigan. Analytical precision (2 sigma) is ±0.1‰. The stable carbon and oxygen isotope values are reported in the conventional δ notation in per mil (‰) relative to Vienna Pee Dee Belemnite (VPDB) and Vienna Standard Mean Ocean Water (VSMOW), respectively. Radiocarbon analyses were performed on a 3MV accelerator mass spectrometer (AMS) at André E. Lalonde AMS Laboratory in Ottawa, Canada. Detailed radiocarbon methods are provided as Supplementary Material.

2.4.5. Specific surface area

Consistent with the methods of Stubbs et al. (2022), a N_2 adsorption method was used to determine Brunauer-Emmett Teller (BET) specific surface areas at Trent University. Samples were first degassed overnight on a Smart VacPrepTM 067 (Micromeritics, Norcross, GA, USA) that slowly heats to and holds them at 200 °C for 10 h under vacuum. BET analysis was performed at 77 K on the Micromeritics TriStar II Plus adsorption unit (Micromeritics, Norcross, GA, USA) and N_2 isotherms were acquired using a P/P0 range of 0.01–0.90. All data processing was done using MicroActive Interactive software (Micromeritics, Norcross, GA, USA).

Table 2
Quantitative mineralogical compositions of powdered rocks as determined with Rietveld refinement using XRD data. BET specific surface (initial) areas and median particle sizes are provided.

Powdered rocks	Mineral abundances (wt%)	BET (m^2/g)	D50 (μm)
Brucite	82.8 wt% brucite; 6.1 wt% hydromagnesite; 5.1 wt% dolomite; 2.5 wt % forsterite; 2.0 wt% magnetite; 0.6 wt% pyroaurite; 0.5 wt% clinochlore; 0.4 wt% lizardite; 0.2 wt% quartz	5.29	8
Wollastonite skarn	38.8 wt% diopside; 20.1 wt% wollastonite; 13.8 wt% orthoclase; 10.1 wt% albite; 8.6 wt% quartz; 2.9 wt% magnesite; 2.8 wt% calcite; 2.1 wt% enstatite; 0.8 wt% biotite	0.87	52
Serpentinite	95.7 wt% lizardite; 4.3 wt% magnetite	64.51	100

3. Results

3.1. Weathering experiments

Wollastonite skarn and brucite powders were cemented after 1 yr of weathering, however, no visual changes were observed in the serpentinite samples. The TIC of wollastonite skarn samples continuously increased from 0.22% ($n = 3$) to 1.01% after 12 months (Fig. 3A). The $\delta^{13}C$ values of the carbonates decreased from −6.2‰ to −17.7‰ and the $\delta^{18}O$ values increased from 21.0‰ to 23.0‰ (Fig. 3B) from 0 to 12 months. Brucite also showed a substantial increase in TIC from initial measurements of 1.22% to 5.98% at 12 months (Fig. 3A). The $\delta^{13}C$ values of the carbonates decreased by −2.9‰ and $\delta^{18}O$ values increased by +10.6‰ from 0 to 12 months (Fig. 3B; Table 4). The $F^{14}C$ values for carbonates in the initial wollastonite skarn and brucite powders were 0.23 and 0.39 respectively while final $F^{14}C$ values were 0.75 and 0.94, respectively. In comparison to initial samples, XRD patterns showed an increase in the intensity of peaks at 29.4° 2θ and 17.6° 2θ (CuKα) that indicates an increase in the amount of calcite and hydromagnesite in the wollastonite skarn and brucite samples, respectively. Serpentinite samples had negligible changes in TIC after 1 yr as values increased and decreased but remained below the detection limit. Due to low carbon content, these samples were not analyzed for their isotopic compositions.

Table 3
Quantitative mineralogical compositions of the experimental kimberlite residues as determined with Rietveld refinement using XRD data. Quantification of blue ground and yellow ground was determined with QEMSCAN. Minerals identified include Cal – calcite, Di – diopside, Or – Orthoclase, Phl – phlogopite, Clc – Clinochlore, Talc, Qtz – quartz, Tr- tremolite, Ab – albite, Lz – lizardite, Sme – smectite, Brc – brucite, Dol – dolomite, Mt. – magnetite, Ap – apatite, Ol – olivine, and Ilm – Ilmenite. R_{wp} is the weighted profile residual, a function of the least squares residual (%). Minerals not detected are indicated by n.d. BET specific surface areas and median particle sizes are provided.

Sample	BET (m^2/g)	D50 (μm)	Cal	Di	Or	Phl	Clc	Talc	Qtz	Tr	Ab	Lz	Sme	Brc	Dol	Mt	Ap	Ol	Ilm	R_{wp} (%)
17VEN-FRD1-P1-K	10.2	520	3.8	14.3	2	6.9	6.3	3.3	2.4	8.3	3.7	19	30.2	n. d.	n. d.	n. d.	n. d.	n. d.	n. d.	8.1
17VEN-FRD2-Cyclone Sample B	7.7	550	4.9	9.8	4.2	17.8	4.7	4.6	4	5.1	7.2	19	18.8	n. d.	n. d.	n. d.	n. d.	n. d.	n. d.	12.4
K01 DVK2	9.8	110	4.4	10.9	n.d.	15.5	3.8	n.d.	1	n. d.	n.d.	26.3	35.9	0.8	0.6	0.5	0.6	n. d.	n. d.	n.d.
2018 DVK	18.3	140	4.4	15.6	n.d.	16.6	n.d.	n.d.	n. d.	2.3	n.d.	33.1	28.1	n. d.	n. d.	n. d.	n. d.	n. d.	n. d.	10.4
Blue ground	n.d.	n.d.	1.7	25.3	4.6	21.2	12.6	0.2	0.1	0.1	33	n.d.	n.d.	n. d.	0.1	0.3	n. d.	0.2	0.6	n.d.
Yellow ground	n.d.	n.d.	3.1	11.7	13.3	35.6	17.8	0.2	1	0.1	15.2	n.d.	n.d.	n. d.	n. d.	0.3	0.1	0.6	1.1	n.d.

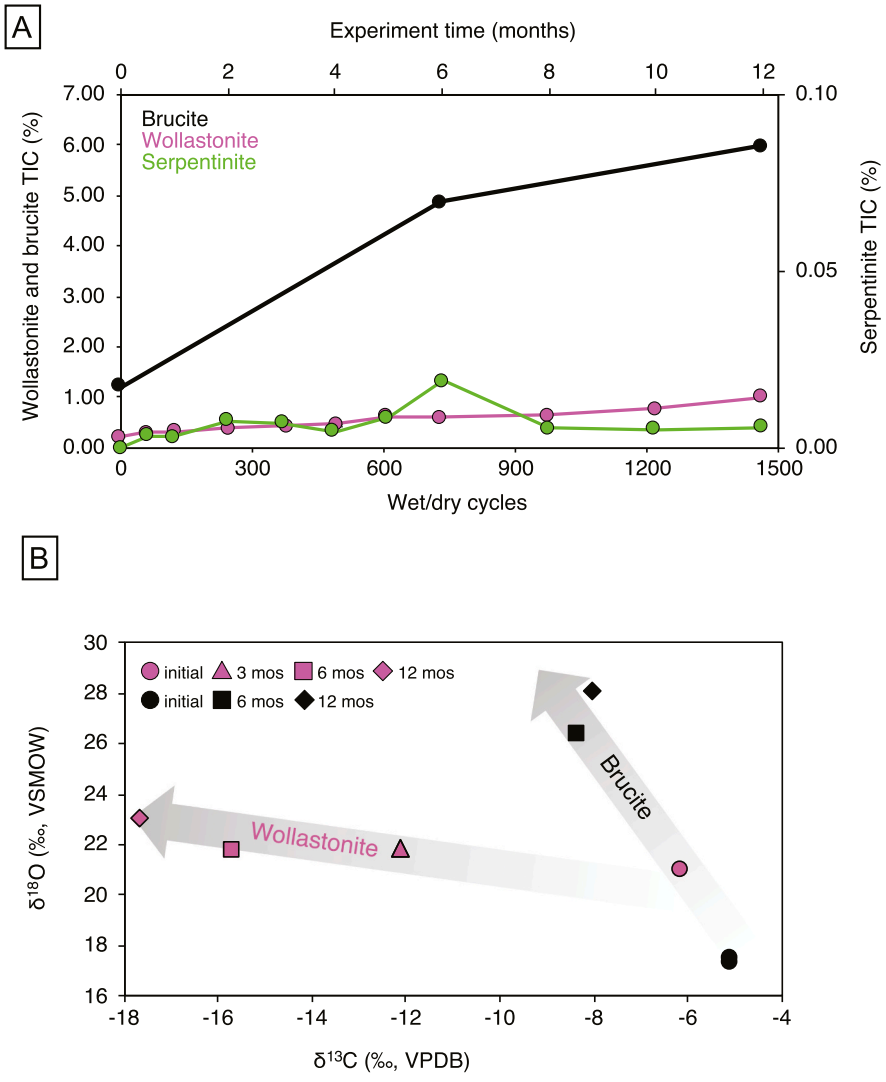

Fig. 3. A: TIC (%) over 1 yr of wetting and dry cycles for brucite, wollastonite, and serpentinite. Error bars, based on analytical error, are smaller than symbols. The standard deviation was not calculated for brucite due to limited samples in this experiment. B: Stable carbon and oxygen isotopic compositions ($\delta^{18}O$ vs. $\delta^{13}C$) for carbonate minerals in wollastonite and brucite experiments after 1 yr of wetting and drying cycles. Serpentinite samples were not analyzed due to low carbon content. Circles represent initial samples, triangles represent 3-month samples, squares represent 6-month samples, and diamonds represent 12-month samples.

Table 4
Initial and final TIC, $\delta^{13}C_{VPDB}$ (‰), and $F^{14}C$ values for experimental samples. Serpentinite samples were not analyzed for isotopes due to low carbon content. (n.a. indicates not analyzed).

Sample	TIC (%)		$\delta^{13}C_{VPDB}$ (‰)		$F^{14}C$	
	Initial	Final	Initial	Final	Initial	Final
17VEN-FRD1-P1-K	0.46	0.48	−5.4	−2.2	0.12	0.39
17VEN-FRD2-Cyclone-SampleB	0.46	0.45	−5.5	−3.1	n.a.	n.a.
K01 DVK2	0.87	0.87	−4.5	−3.7	n.a.	n.a.
2018 DVK	0.43	0.45	−6.8	−1.1	0.16	0.44
Brucite	1.22	5.98	−5.1	−8.0	0.39	0.94
Wollastonite skarn	0.22	1.01	−6.2	−17.7	0.23	0.75
Serpentinite	0.00	0.00	n.a.	n.a.	n.a.	n.a.

The kimberlite residues are a diverse mixture of non-carbonate and carbonate minerals that are cation sources for secondary carbonate precipitation (Table 3). White efflorescences were visible on the top surfaces of the kimberlite residues after 1 month of wetting and drying cycles (Fig. S1). XRD analysis of 17VEN-FRD2-SampleB and K01 DVK2 showed that the dominant secondary phase in the efflorescences was trona [$Na_3(CO_3)(HCO_3)\cdot 2H_2O$]. SEM and EDS results of the secondary precipitates confirm XRD and are available in the Supplementary Material.

TIC content of the 17VEN-FRD1-P1K residues increased from 0.46% to 0.54% during 0 to 6 months of wetting and drying (Fig. 4) before decreasing to 0.48% C by 12 months. Similarly, 17VEN-FRD2-SampleB residues increased from 0.46 to 0.48% C by 3 months and decreased to 0.45% C by 12 months (Fig. 4). The K01 DVK2 sample had a substantially greater initial TIC content of 0.87% C than the other kimberlite samples and increased to 0.89% C after 2 weeks before declining to initial measurements (0.87% TIC) by 12 months (Fig. 4). The TIC in 2018 DVK increased from 0.43 to 0.45% C between 0 and 6 months and did not exhibit any changes for the remainder of the experiments (Fig. 4).

The $\delta^{13}C$ and $\delta^{18}O$ values of the suite of Venetia kimberlite samples ($n = 14$) ranged from −5.5‰ to −4.5‰ and 14.7‰ to 17.3‰, respectively (Fig. 5A). The isotopic compositions of samples 17VEN-FRD1-P1K, 17VEN-FRD2-SampleB, K01 DVK2, and 2018 DVK were analyzed during the wet-dry cycling experiments. After 12 months, the $\delta^{13}C$ values of these samples increased on average ($n = 2$) by +3.2‰, +2.4‰, +0.8‰, and + 5.6‰, respectively, following a linear trend (Table 4 and Fig. 5B). The $\delta^{18}O$ values of 17VEN-FRD1-P1K and 17VEN-FRD2-SampleB increased on average (n = 2) by +3.6‰ and + 3.0‰; however, those for K01 DVK2 decreased by −0.1‰ by 12 months, despite increases measured at 3 and 6 months (Fig. 5B). The $F^{14}C$ values for carbonate minerals in the kimberlite residues were 0.117 and 0.161 for initial 17VEN-FRD1-P1K and 2018 DVK and 0.387 and 0.436 after 12 months of weathering, respectively (Table 4).

3.2. Blue and yellow ground

Blue and yellow ground kimberlite samples were characterized to investigate long-term kimberlite weathering in the context of CO_2 mineralization. These samples were mineralogically similar to the Venetia residues with major abundancies of silicate minerals (e.g., serpentine, smectite, olivine and diopside) and minor abundances of carbonates (e.g., calcite). The blue ground was dark and competent as it had not been exposed to weathering (Fig. 6A). The yellow ground was shades of light brown and yellow and was very fragile and friable, with

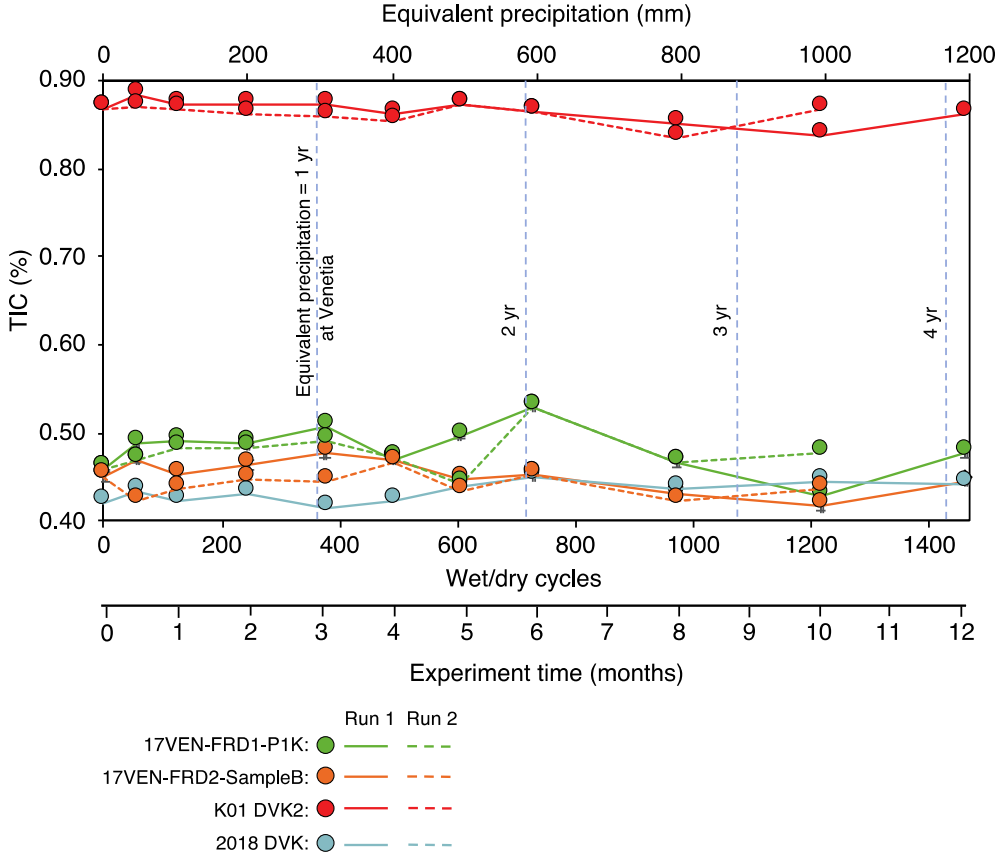

Fig. 4. TIC over 1 yr of wetting and drying cycles for 17VEN-FRD1-P1K, 17VEN-FRD2-SampleB, K01 DVK2, and 2018 DVK. Error bars of the TIC measurements (analytical error) are smaller than the symbols used. Dashed, vertical blue lines represent equivalent rainfall at Venetia for 1 to 4 years. Coloured dashed lines denote duplicate samples. (For interpretation of the references to colour in this figure legend, the reader is referred to the web version of this article.)

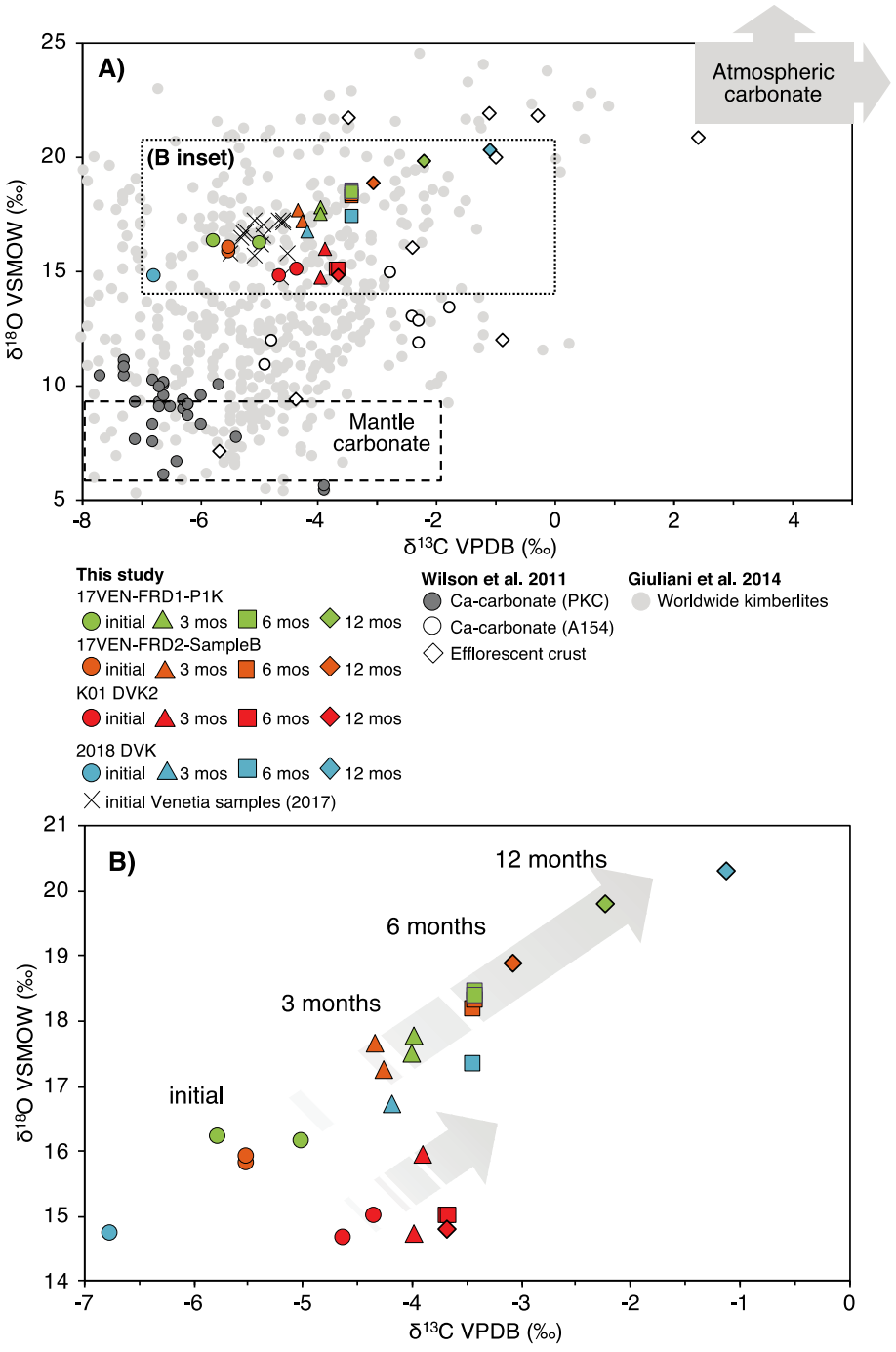

Fig. 5. Stable carbon ($\delta^{13}C_{VPDB}$) and oxygen ($\delta^{18}O_{VSMOW}$) isotopic compositions of kimberlites. A: Worldwide kimberlites (Giuliani et al., 2014) and kimberlite from the Diavik Diamond Mine (Canada) and carbonate efflorescences (Wilson et al., 2011) plotted with Venetia and laboratory weathered kimberlite samples (B inset). The dashed box on the bottom left represents a mantle carbonate range (Giuliani et al., 2014) and the grey box on the top right corner represents the atmospheric carbonate range (Wilson et al., 2011). B: Isotopic shift of laboratory weathered kimberlites after 3, 6, and 12 months of wetting and drying cycles. Measurement errors (2σ) are smaller than the symbols employed.

distinctive secondary carbonate minerals visible on the surface of the rock (Fig. 6B). TIC content of the blue ground ($n = 9$) ranged from 0.52% to 3.60%, intermediately weathered kimberlite ($n = 2$) ranged from 0.62% to 1.15%, and yellow ground ($n = 20$) ranged from 0.69% to 3.43%. Surface carbonate coatings composed of pure calcite that were sampled from the yellow ground were assumed to contain 12% C by weight (Fig. 7B–C). There were insufficient masses of carbonate coatings for TIC analyses.

The $\delta^{13}C$ values of the blue ground ranged from −7.2‰ to −4.6‰ and $\delta^{18}O$ values ranged from 11.5‰ to 13.6‰. Yellow ground $\delta^{13}C$ values ranged from −7.0‰ to −5.1‰ with $\delta^{18}O$ values ranging from 15.4‰ to 22.8‰. The $\delta^{13}C$ values of carbonate surface coatings that were selectively sampled ranged from −8.2‰ to −6.0‰ and $\delta^{18}O$ values ranged from 15.3‰ to 27.0‰. The $\delta^{13}C$ values for intermediately weathered kimberlite ranged from −6.4‰ to −5.8‰ and the $\delta^{18}O$ values ranged from 12.6‰ to 12.7‰ (Fig. 7A–C). The $F^{14}C$ values for carbonate minerals in the blue and yellow ground were 0.052 and 0.032, respectively (Table 4).

QEMSCAN analysis showed there was twice as much calcite in the yellow ground (3.1 wt%) as compared to the blue ground (1.7 wt%; Fig. 8). Calculated calcite abundances based on TIC contents were much greater than those obtained with QEMSCAN, although they also indicated there was twice as much calcite in the yellow ground (15 wt%) compared to the blue ground (7 wt%). The difference in the QEMSCAN and TIC-based calcite abundances is likely due to the finely disseminated nature of calcite throughout the yellow ground, which QEMSCAN could not quantify. However, QEMSCAN provides valuable textural information. Most of the calcite in the yellow ground was present as stringers or

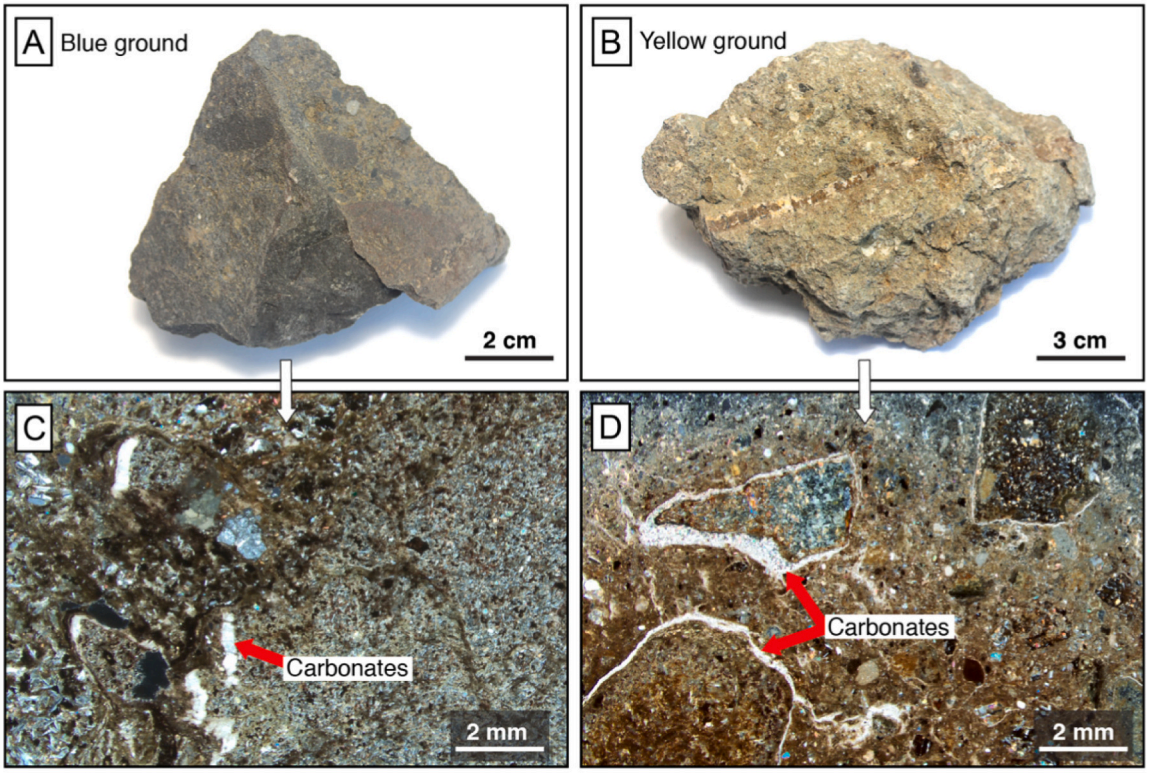

Fig. 6. Photographs of kimberlite rock from the Voorspoed Diamond Mine, South Africa. A-B: Hand specimens of blue ground (unweathered kimberlite) and yellow ground (weathered kimberlite). C and D: Thin section micrographs of blue and yellow ground samples under cross-polarized light, respectively. Carbonate veinlets (arrows) surround larger grains in the yellow ground. Red arrows indicate carbonate minerals. (For interpretation of the references to colour in this figure legend, the reader is referred to the web version of this article.)

veinlets, whereas the blue ground contained discreet calcite grains. Calcite veinlets commonly appeared surrounding coarse grains and in fractures. Petrographic thin sections of yellow ground show large carbonate veinlets running through the kimberlite opposed to low carbonate content in the blue ground (Fig. 6C–D).

4. Discussion

4.1. Reaction pathways during weathering

Two main reaction pathways were identified from experiments: 1) non-carbonate dissolution and 2) primary carbonate dissolution (Fig. 9). The first pathway has two potential outcomes: atmospheric CO_2 is sequestered within new carbonate minerals (pathway 1A; desirable for CO_2 sequestration), or there is no change in CO_2 content due to formation of new non-carbonate minerals such as clay minerals or sulfates (pathway 1B; undesirable). Both pathways may be accompanied by changes in TIC and carbon isotopic compositions. Experiments using brucite, wollastonite skarn, and serpentinite were dominated by pathway 1A.

The second pathway has five possible outcomes (pathways 2A through 2E), all considered undesirable for carbon removal. These outcomes could result in either CO_2 being retained, exchanged with the atmosphere, or lost during precipitation of sulphates or clay minerals. Carbonate mineral dissolution can result in the same carbonate mineral being formed either from recycled CO_2 (2A) or atmospheric CO_2 that is exchanged with CO_2 in the pore fluids (2B). Neither outcome results in net carbon removal; however, the latter outcome (2B) may affect the isotopic compositions of the carbonate minerals. Similarly, carbonate mineral dissolution can result in the formation of a different carbonate mineral with CO_2 either retained (2C) or exchanged with the atmosphere (2D; the dominant scenario for kimberlite) with the result potentially being a different TIC content. Although not observed in this study, the final potential pathway results in a loss of CO_2 when there is the precipitation of non-carbonate minerals (e.g., clay minerals or sulfates; 2E). Although these pathways are not desirable for CO_2 sequestration, they have important effects on carbon cycling during rock weathering with implications for verification of CO_2 removal.

4.1.1. Brucite, wollastonite skarn and serpentinite weathering reactions

Brucite is highly reactive with CO_2 and is considered a source of easily extractable (labile) Mg (Vanderzee et al., 2019). In the weathering experiments, brucite showed a net increase in TIC (+4.76%) which was the greatest observed in all experiments. Secondary carbonates that formed on the surface of the brucite were identified as hydromagnesite (Eqs. (1)–(2)) resulting in a net gain in CO_2 (pathway 1A) which is consistent with other studies (Harrison et al., 2015; Harrison et al., 2013; Power et al., 2021, and references therein). Specifically, various mining environments produce secondary efflorescences including Mount Keith, where hydromagnesite forms via brucite carbonation (Wilson et al., 2014) and Clinton Creek and Cassiar where silicate weathering results in the formation of hydrated Mg-carbonate minerals (Wilson et al., 2009a). This reaction pathway is the most favoured for passive carbonation as it results in a net removal of CO_2 (pathway 1A).

$$Mg(OH)_2 + CO_2 \rightarrow Mg^{2+} + CO_3^{2-} + H_2O \quad (1)$$

$$5Mg^{2+} + 4CO_3^{2-} + 2OH^- + 4H_2O \rightarrow Mg_5(CO_3)_4(OH)_2{\cdot}4H_2O \quad (2)$$

The log dissolution rate of brucite is −11.5 mol/cm^2/s at the pH of deionized water used in experiments (pH = 5.6; Pokrovsky and Schott, 2004), which is orders of magnitude faster than the rates of other minerals tested in this study. Faster mineral dissolution results in greater pH buffering, leading to a greater drawdown of atmospheric CO_2. Stubbs et al. (2022) measured CO_2 fluxes between the atmosphere and a variety

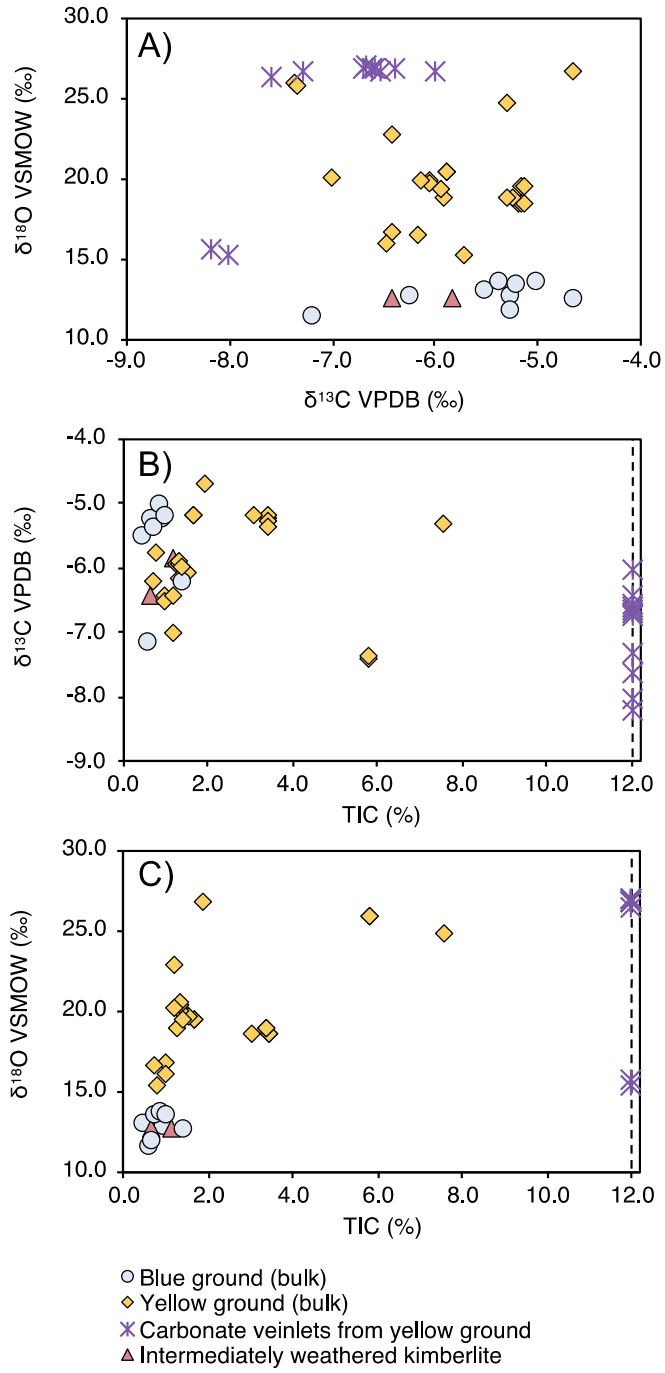

Fig. 7. Stable carbon ($\delta^{13}C_{VPDB}$) and oxygen ($\delta^{18}O_{VSMOW}$) isotopic compositions and TIC of kimberlite specimens from the Voorspoed Diamond Mine, South Africa, including bulk samples of blue ground, intermediately weathered kimberlite, and yellow ground, and carbonate veinlets that were selectively sampled from the yellow ground. A: $\delta^{18}O$ versus $\delta^{13}C$. B: $\delta^{13}C$ versus TIC. C: $\delta^{18}O$ versus TIC. Black dashed lines represent pure calcite (12% C) for the carbonate veinlets. (For interpretation of the references to colour in this figure legend, the reader is referred to the web version of this article.)

of mineral feedstocks, including brucite from the same source used here, and found that the greatest CO_2 removal rates were achieved using materials with the fastest mineral dissolution rates. The rate of TIC increase was rapid during the first 6 months, and then declined during the remainder of the experiment (Fig. 3A). This change in carbonation rate indicates that brucite was being consumed by the reaction and suggests brucite surfaces may also have become passivated (Harrison et al., 2015). In dissolution/precipitation studies such as this, as well as carbonation in aqueous solutions, the degree of brucite carbonation is almost always limited by CO_2 supply (Harrison et al., 2013; Power et al., 2016).

The wollastonite skarn contained a greater abundance of diopside (38.8 wt%) than wollastonite skarn (20.1 wt%); however, the latter mineral dissolves much more quickly: log dissolution rate = −12.5 mol/cm^2/s at pH 5.6 (Pokrovsky et al., 2009) compared to diopside at −15.0 mol/cm^2/s (Declercq and Oelkers, 2014). Thus, wollastonite skarn was expected to be the primary source of calcium for carbonate precipitation (Stubbs et al., 2022), which resulted in a TIC increase of 0.79% C. Aqueous carbonation studies have reported that wollastonite rapidly carbonates compared to Mg-silicates (Huijgen et al., 2006), similar to what was observed in these dissolution/ precipitation experiments. The dissolution of wollastonite skarn and subsequent reaction with dissolved CO_2 caused the formation of calcite (Eqs. (3)–(4)), consistent with other studies (Daval et al., 2010; Haque et al., 2019). For example, wollastonite skarn has a CO_2 sequestration capacity of 44 g CO_2 per 116 g wollastonite skarn (Tai et al., 2006), therefore a total of 40 Mt. of CO_2 could be stored in world's wollastonite skarn reserve of at least 100 Mt. (Haque et al., 2019; USGS, 2020).

$$CaSiO_3 + CO_2 + 2H_2O \rightarrow Ca^{2+} + CO_3^{2-} + H_4SiO_4 \quad (3)$$

$$Ca^{2+} + CO_3^{2-} \rightarrow CaCO_3 \quad (4)$$

Weathering of serpentine during experiments resulted in an insignificant increase in TIC (+0.02% from 0 to 6 months), which is likely within measurement error of a 0% overall increase. Furthermore, no secondary precipitates were observed on serpentine surfaces and no carbonate minerals were detected using XRD. Despite the negligible TIC changes in this experiment, previous studies have observed precipitation of secondary carbonate minerals during serpentinite weathering (Eq. (5); Wilson et al., 2009a) where hydrated Mg-carbonates are a stable sink for CO_2.

$$Mg_3Si_2O_5(OH)_4 + 3CO_2 + 2H_2O \rightarrow 3\,Mg^{2+} + 3CO_3^{2-} + 2H_4SiO_4 \quad (5)$$

The log dissolution rate of chrysotile, a serpentine group mineral, is −15.5 mol/cm^2/s at a pH of 5.6 (Thom et al., 2013), which is substantially slower than the rates for brucite and wollastonite skarn. However, serpentine has a much faster initial dissolution rate where labile cations on the mineral surface are released into solution quickly and supply required Mg for carbonate precipitation (Power et al., 2020; Vanderzee et al., 2019). In this study the serpentinite, which is dominated by lizardite (95.7 wt%), had the greatest surface area available for reaction. If the serpentinite was dominated by chrysotile this would have been increased even further as there is also surface area in its lumen space.

The carbonation rate (Eq. (6)) was calculated for brucite and wollastonite skarn after 1 year of weathering:

$$Carbonation\ rate\ (kg\ CO_2/t\ mineral/yr) = \frac{\left(\frac{TIC_f - TIC_i}{100\%}\right) \times \left(\frac{M_{CO_2}}{M_C}\right) \times \left(\frac{100\ wt.\%}{mineral\ wt.\%}\right) \times \left(\frac{1000\ kg}{1\ t\ mineral}\right)}{t} \quad (6)$$

where TIC_f and TIC_i are the final and initial TIC contents (% C), respectively, M_{CO_2} and M_C are the molar masses of CO_2 and C (g/mol), respectively, mineral wt% is the abundance of the mineral of interest, and t is time (yr). Brucite and wollastonite skarn had carbonation rates of 212 kg CO_2/t brc/yr and 145 kg CO_2/t wol/yr, respectively (Table 5). These rates are consistent with other studies investigating the carbonation potential of identical feedstocks. Based on the CO_2 removal rates in brucite reported by Wilson et al. (2014) approximately 145–360 kg CO_2/t brc/yr are removed at Mount Keith Nickel mine. Haque et al. (2019) tested the use of wollastonite skarn in soil for both CO_2 sequestration and plant growth and estimated that approximately 145 kg CO_2/t soil with wol/yr are removed, similar to this study. No carbonation rate was calculated for serpentine due to the negligible changes in TIC.

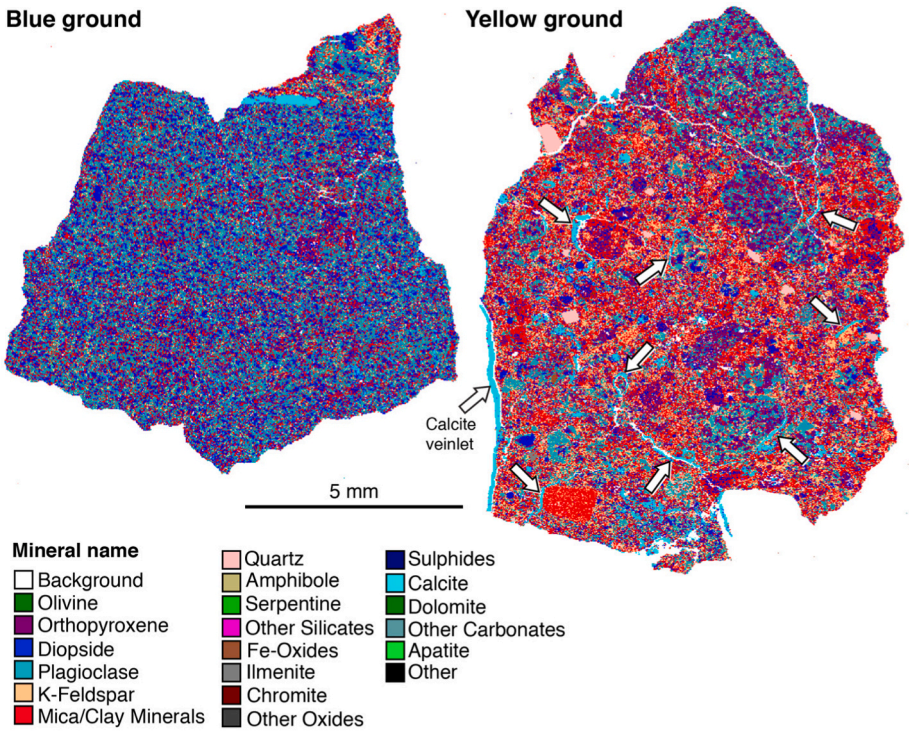

Fig. 8. QEMSCAN images of blue (left) and yellow (right) ground. Calcite is shown in a teal colour in both images. Carbonate (calcite) veinlets (indicated by arrows) are found within fractures or have formed around coarser particles which is a result of secondary mineralization from fluids. (For interpretation of the references to colour in this figure legend, the reader is referred to the web version of this article.)

4.1.2. Kimberlite weathering reactions

Changes in TIC were variable within the kimberlite, with increases in TIC measured up to 6 months, reaching a maximum CO_2 removal rate of 2.6 kg CO_2/ t kimberlite/ yr (Table 5) before declining again later in the experiment. The early TIC increases were likely caused by the rapid initial dissolution of lizardite, diopside and clinochlore, owing to the presence of labile cations on mineral surfaces as previously described for the weathering of serpentine (Lu et al., 2022; Power et al., 2020; Vanderzee et al., 2019). After the supply of labile surface cations was exhausted, reaction of the recalcitrant bulk of the silicate minerals did not result in a measurable increase in TIC during the remainder of the experiment. After more exposure to wetting periods, the carbonate minerals that had formed (i.e., trona) likely dissolved due to their instability.

TIC decreases may result from the dissolution of pre-existing carbonate minerals that have a favorable ratio between cations and anions, such as calcite or magnesite (1,1 Me:CO_2, where Me = Ca or Mg) and subsequent precipitation of a carbonate mineral with a lower TIC content (pathway 2D) on a per mole basis. Because trona has a lower TIC content (10.6 wt%) compared to pre-existing calcite (12 wt%), CO_2 must either be retained from the dissolution of the pre-existing calcite (pathway 2C) or exchanged with atmospheric CO_2 (pathway 2D) during formation of trona. In another example, if pre-existing magnesite in mine residues dissolved it would release Mg and C and could reprecipitate as hydromagnesite, which is hydrated and has a 5:4 ratio of Mg:CO_2 (Power et al., 2017), resulting in a lower TIC value. In the experiments reported here, addition of water promotes mineral dissolution and is wicked up through capillary forces towards the surface where it evaporates to precipitate efflorescences of secondary minerals. These evaporites appear and disappear over time, however, there are not substantial changes in TIC, implying that C is likely retained (pathway 2A).

The majority of minerals present in the kimberlite residues are dominantly Ca- and Mg-bearing, with the exception of saponite, which also contains interlayer Na at Venetia. Consequently, the cations present in trona are likely sourced from saponite. Zeyen et al. (2022) examined how the cation exchange capacity of smectites can be used for mineral carbonation whereby labile interlayer cations of interest (e.g., Ca^{2+}) are exchanged for less desirable cations (e.g., Na^{+}, K^{+}) present in solution. Following this process, the available cations may react with dissolved inorganic carbon to form secondary carbonate minerals. Zeyen et al. (2022) tested Venetia kimberlite and found high Na extraction (2.82–3.93 g/kg) occurred, indicating that saponite present in these residues is a source of Na for carbonate precipitation.

The last pathway shown in Fig. 9 involves the precipitation of non-carbonate minerals such as clays or sulphates (pathway 2E). At Venetia, sulphates were seen on the surface of the FRD which is not favorable for CO_2 sequestration as these minerals act as non-carbonate sinks for cations. It is possible that sulphate efflorescences formed in the latter half of the experiment at abundances that were too low to be detected by XRD yet sufficiently high to decrease TIC content.

For the kimberlite residues, carbonate dissolution likely dominated (pathway 2) compared to non-carbonate dissolution (pathway 1) in the other experiments. Although the calcite abundance (3.8–4.7 wt%) in the residues was relatively low compared to the abundances of most silicate minerals, the dissolution rate of calcite is orders of magnitude faster. For instance, the log dissolution rate of calcite at the same pH of water used in experiments is −9.7 mol/cm^2/s while the rates for diopside, lizardite, and clinochlore are −15.0, −15.5, and − 17.0 mol/cm^2/s, respectively (Declercq and Oelkers, 2014). Carbonates in the residues neutralized the acidity of the water (pH 5.6), limiting silicate dissolution that would otherwise occur in the absence of the more reactive carbonate minerals. In these experiments, water could not drain from the vials, resulting in constant carbonate cycling; thus, carbonate, Mg and Ca were continuously cycled between solution and solid, never being removed from the vials to better expose silicate minerals to weathering.

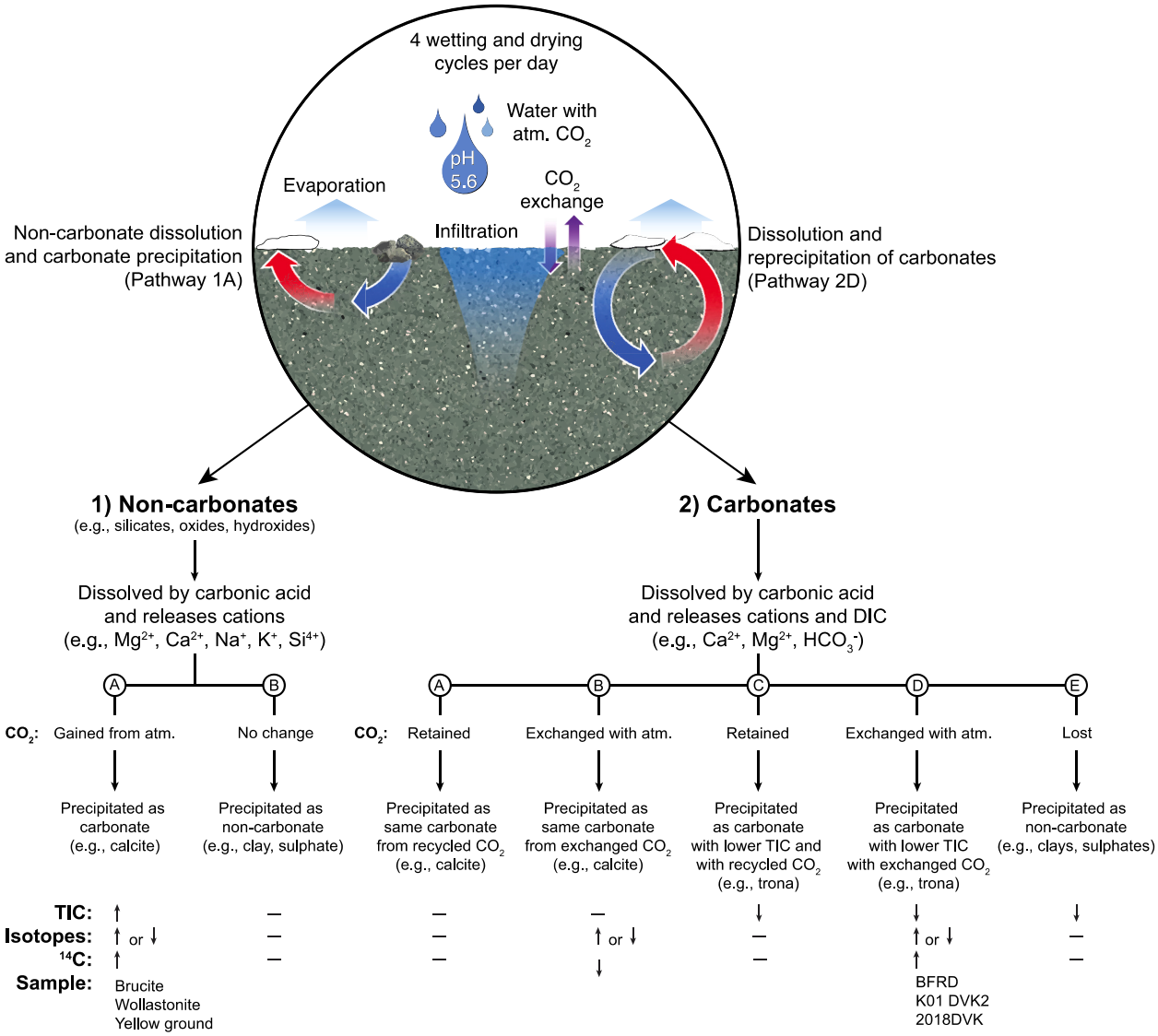

Fig. 9. Conceptual diagram illustrating fundamental processes occurring during weathering experiments. Four wet-dry cycles occurred per day where water infiltration (pH = 5.6) promoted mineral dissolution of non-carbonate and carbonate minerals and evaporation drove the precipitation of secondary carbonate minerals. Carbonate dissolution and reprecipitation likely resulted in CO_2 exchange where there was no net gain in atmospheric CO_2. The flow diagram outlines potential reaction pathways when sourced from non-carbonates (left branch) versus carbonates (right branch) during weathering. Possible effects on TIC and $\delta^{13}C$ and $\delta^{18}O$ values are shown using ↑ (increase), ↓ (decrease) and – (no change). Brucite, wollastonite, and serpentinite are dominated by non-carbonate dissolution and precipitation of carbonates (1A) while kimberlite residues are dominated by dissolution and reprecipitation of carbonates with CO_2 exchange from the atmosphere (2D).

Table 5
Maximum carbonation rates (kg CO_2/ t sample/ year) for the different feedstocks tested.

Sample name	CO_2 removal rate (kg CO_2/ t sample/ yr)
Brucite	212
Wollastonite	145
Serpentinite	0
Kimberlite	2.6

4.1.3. Changes in isotopic compositions during weathering experiments

Atmospheric CO_2 and pre-existing carbonate minerals were the only carbon sources in the experiments; other carbon sources, such as organics, were absent. Many processes and environmental factors may affect the isotopic compositions of carbonate minerals including mineral dissolution and precipitation, carbon cycling between primary carbonate and atmospheric sources, and the temperature of formation. Thus, deciphering isotopic compositions to assess CO_2 sequestration in complex environments is challenging. The experiments in this study offer an opportunity to interpret the isotopic compositions of carbonate minerals formed under relatively simple conditions (e.g., room temperature) with few carbon sources and sinks.

4.1.3.1. Brucite weathering. Despite a substantial increase in TIC and formation of hydromagnesite, there was a decrease in $\delta^{13}C$ values by −2.9‰ after 1 yr. Dypingite [$Mg_5(CO_3)_4(OH)_2{\cdot}5H_2O$] can transform to hydromagnesite and may have been the initial precipitate in experiments (Harrison et al., 2015). If dypingite precipitates at equilibrium with atmospheric CO_2, it would have a $\delta^{13}C$ value of approximately 4.1‰ rather than −2.9‰ [using fractionation factors from Harrison et al. (2021) and Mook et al. (1974) and $\delta^{13}C = -8.5$‰ for atmospheric CO_2]. The $\delta^{18}O$ values were more enriched in the brucite (28.1‰) compared to the wollastonite (23.0‰) which is likely a result of more O

from H_2O being consumed in the hydromagnesite into the CO_3, OH, and H_2O. This amplifies the evaporative signal compared to what is seen in calcite from the wollastonite experiments. These data indicate that the hydromagnesite (or dypingite) did not form in equilibrium with atmospheric CO_2.

However, the increase in TIC unequivocally demonstrations removal of CO_2 and radiocarbon analysis confirms it is modern atmospheric CO_2 with $F^{14}C$ increasing from 0.39 to 0.94 over the course of the experiment. The $F^{14}C$ of atmospheric CO_2 is currently 1.01 (Hua et al., 2022), so the greater the amount of modern atmospheric CO_2 incorporated into a mineral, the greater its $F^{14}C$ value. Similarly, Wilson et al. (2010) found that $\delta^{13}C$ values decreased during the carbonation of brucite to form dypingite which demonstrated that carbonation outpaced CO_2 uptake into solution; thus, reactions were CO_2 limited. Given the relatively fast carbonation rates of brucite (Harrison et al., 2013), the depletion in ^{13}C was likely a result of a kinetic isotope fractionation effect whereby carbonation was limited by the supply of atmospheric CO_2 into pore waters (Wilson et al., 2010). Consequently, carbonate minerals were not precipitated at equilibrium with atmospheric CO_2. It is not possible to conclusively fingerprint drawdown of atmospheric CO_2 from the $\delta^{13}C$ values of the secondary carbonate minerals, thus we recommend that stable isotopes not be used as a sole means of monitoring or confirming carbon storage.

4.1.3.2. Wollastonite skarn weathering. Wollastonite weathering also caused a decrease in $\delta^{13}C$ values by −11.5‰ in 1 yr despite the increase in TIC (+0.79%; Fig. 3) and the detection of newly formed calcite. Radiocarbon analyses showed an increase in $F^{14}C$ from 0.23 to 0.75, confirming drawdown of atmospheric CO_2. Other studies have documented negative trends in $\delta^{13}C$ values during carbonation (Harrison et al., 2013) however, there is limited published research on kinetic isotope fractionation occurring during wollastonite skarn carbonation (Peck et al., 2023). The equilibrium carbon isotope fractionation between calcite and HCO_3^- at room temperature is +2‰ (Deines et al., 1974), which means that calcite precipitated at equilibrium with atmospheric CO_2 should have a $\delta^{13}C$ value of approximately 1.5‰ rather than −17.7‰. The $\delta^{13}C$ values are much more negative than brucite (−8.0‰) which may be caused by the formation of calcite crusts. Upon the completion of experiments the wollastonite was heavily cemented by calcite whereas the brucite was cemented by hydromagnesite, but to a lesser extent. It is likely that the latter was more permissive of CO_2 ingress compared to calcite given the difference in physical properties and carbonate composition. These data indicate that these secondary minerals are not forming in isotopic equilibrium. Consistent with the brucite interpretation, stable isotope data cannot be used to verify atmospheric CO_2 sequestration and should be coupled with radiocarbon analysis.

4.1.3.3. Kimberlite residue weathering. The stable isotopic composition of carbonates within the Venetia samples (Fig. 6A) falls within the broad range of isotope values of other kimberlites compiled by Giuliani et al. (2014) in southern Africa (Deines and Gold, 1973; Kirkley et al., 1989; Kobelski et al., 1979; Sheppard and Dawson, 1975), Kenya (Ito, 1986), North America (Arima and Kerrien, 1988; Deines and Gold, 1973; Fedortchouk and Canil, 2004; Price et al., 2000; Wilson et al., 2007), Russia (Galimov and Ukhanov, 1989; Kamenetsky et al., 2012; Kuleshov and Ilupin, 1983; Ustinov et al., 1994), and Greenland (Tappe et al., 2011). Kimberlitic carbonates may have $\delta^{13}C$ and $\delta^{18}O$ compositions that are similar to other materials derived from the mantle. However, the isotopic composition of kimberlites may also reflect the incorporation of sedimentary carbonate minerals and organics during kimberlite emplacement as well as post-emplacement alteration by hydrothermal and meteoric fluids as well as CO_2 degassing/exsolution (Giuliani et al., 2014). The isotopic compositions of the Venetia carbonates (average $\delta^{13}C$ and $\delta^{18}O$ values of −5.0‰ and 16.4‰) likely reflect a mixture of these various sources.

Numerous studies have noted that isotopic compositions can be altered whether in equilibrium or disequilibrium (Gorski and Fantle, 2017; Harrison et al., 2022; Li et al., 2014; Stamm et al., 2019). In this study the overall decrease in TIC, precipitation of trona, and continuous enrichment in ^{13}C and ^{18}O towards an atmospheric signal confirm that pathway 2D was dominant. In this scenario, an enrichment in ^{13}C occurs because C from the primary carbonate is exchanged with C from the atmosphere and incorporated into secondary phases. Similarly, the reprecipitated carbonate minerals became increasingly enriched in ^{18}O because trona forms as an evaporite from ^{18}O-enriched pore waters and it contains O in multiple sites compared to only one in calcite. The TIC content would still decrease if the newly formed carbonate has a lower C content, but the $\delta^{13}C$ and $\delta^{18}O$ values still increase because it is sequestering C from the atmosphere. Unfortunately, this scenario does not result in a net gain in CO_2 as confirmed by the small but measurable decrease in TIC.

There are other plausible explanations for the increasingly positive $\delta^{13}C$ and $\delta^{18}O$ values of the kimberlite residues, albeit less supported by the data. Over the year of repeated wetting and drying cycles, white efflorescences formed on the surface would dissolve and re-precipitate due to their instability. At 6 months, when there was a substantial increase in TIC, it is possible that calcite had formed via silicate weathering prior to trona forming at around 12 months. Similarly, other studies have observed that (Mg) carbonate phase transformation via mineral dissolution-precipitation processes results in substantial alterations to the isotopic composition (Harrison et al., 2021).

Temperature affects the isotopic composition of carbonate minerals as fractionation factors are temperature dependent (Muhlinghuas et al., 2009). There is less fractionation at higher temperatures than at lower temperatures. In this study, we must consider the two types of carbonate minerals that are present (primary versus secondary), which formed at different temperatures. For example, the original fluid which formed the primary carbonate in the kimberlite rock is going to be different in composition and temperature than the fluid which formed the secondary carbonate in these weathering experiments. Although the formation temperature of the primary carbonates is not known, these temperatures would be much higher than the secondary carbonates which formed at room temperature in the laboratory and may affect the isotopic composition.

4.2. Blue and yellow ground

Kimberlite pipes typically have unweathered bases (blue ground) with weathered kimberlite (yellow ground; da Costa, 1989; Smith et al., 1996; Wagner, 1971) extending from the surface to depths as great as tens of meters (Sarma and Verma, 1996). Weathered kimberlite has a yellow colouration resulting from oxidation and hydration of iron (Sarma and Verma, 1996), whereas blue ground is much darker due to less alteration. While experiments were designed to simulate short-term weathering, the yellow ground provides insights into long-term kimberlite weathering.

As demonstrated by QEMSCAN, most of the calcite in the yellow ground occurred as veinlets or stringers characteristic of secondary mineralization from weathering by fluids, such as meteoric water. In kimberlite bodies, open fractures can allow for the crystallization of secondary minerals, such as calcite, resulting in stringers (Ignatov et al., 2018). The pre-existing calcite detected in blue ground samples suggests there could have been carbonate dissolution and eventually reprecipitation in the yellow ground, similar to the kimberlite weathering experiments (2D). However, the doubling of TIC between blue ground and yellow ground samples suggest that prolonged kimberlite weathering results in detectable CO_2 mineralization, meaning that non-carbonate dissolution must also have been a factor in yellow ground formation.

The stable isotope trends of the yellow ground were similar to those for brucite and wollastonite skarn as yellow ground exhibited depletions in $\delta^{13}C$ (−5.8‰) and enrichments in ^{18}O (18.96‰) with increasing TIC.

One hypothesis is that during precipitation events, rainwater would infiltrate into the kimberlite where secondary carbonates can precipitate in isolation from the atmosphere. This infiltrating fluid has a large pool of oxygen from the water and a miniscule pool of dissolved inorganic carbon from atmospheric CO_2. Thus, calcite precipitation would occur out of equilibrium with atmospheric CO_2, causing a depletion in ^{13}C. This depletion occurs because the uptake of CO_2 into solution is outpaced by the removal of DIC during secondary carbonate formation (Wilson et al., 2010), which in the case of yellow ground are the calcite veinlets. Mixing between the primary carbonate pool, which is much larger, and the atmospheric CO_2 present in meteoric waters will also confound the interpretation of isotope values. In contrast, secondary carbonate minerals are likely to precipitate in equilibrium with water given the large pool of oxygen, resulting in enrichment in ^{18}O (Oskierski et al., 2016). Thus, $\delta^{18}O$ values show an enrichment in yellow ground while there is a small decrease in $\delta^{13}C$ values. The isotopic values of brucite and wollastonite skarn exhibited similar trends caused by C isotopes being out of equilibrium whereas O isotopes were in equilibrium.

A second hypothesis is that the depletion in ^{13}C is due to the incorporation of carbon sourced from soil organic matter (SOM) during weathering to form the yellow ground. For example, Wilson et al. (2011) showed that organic matter causes a depletion in ^{13}C in secondary carbonates in the kimberlite residues at the Diavik Diamond Mine as a result of mineralization of organic wastes deposited in the impoundment. Various shrubs and grasses that require warm growing seasons have $\delta^{13}C$ values ranging from −17‰ to −9‰ with an average value of −13‰ (Farquhar et al., 1989; Lee et al., 2005; O'Leary, 1981). Plant species and SOM at Voorspoed have not been analyzed for their $\delta^{13}C$ values; however, incorporation of carbon derived from these sources into the yellow ground carbonates could explain the ^{13}C depletion relative to the blue ground.

Although the carbonate veinlets and stringers are strong evidence of secondary carbonate precipitation involving meteoric waters, the yellow ground is nearly radiocarbon dead and contains less ^{14}C than the blue ground. It is possible that any ^{14}C mineralized through weathering has decayed over time. For example, given that the yellow ground had twice as much carbon stored in carbonate minerals as the blue ground, and assuming that this additional carbon is modern, there would be approximately 50% modern carbon. With a half-life of 5730 ± 40 for ^{14}C, the portion of modern carbon in the yellow ground would return to similar levels in the blue ground after tens of thousands of years.

4.3. Implications for carbon verification

The weathering experiments in this study using brucite, wollastonite skarn, serpentinite, and kimberlite were evaluated using four carbon verification methods: 1) quantitative mineralogy, 2) total inorganic carbon, 3) stable carbon and oxygen isotopes, and 4) radiocarbon (Table S2). These techniques have advantages and disadvantages and should be used in combination with each other or additional methods.

4.3.1. Quantitative mineralogy

The advantages of using mineralogical analyses by XRD and QEMSCAN are that secondary carbonates (i.e., the CO_2 sinks) are identified as well as the cation sources, which are useful for understanding reaction pathways (Table S2; e.g., Farquhar et al., 2015; Wilson et al., 2009a). However, there are also disadvantages to mineralogical carbon verification, including: 1) the inability to quantify amorphous carbonates by XRD, 2) challenges in distinguishing between primary and secondary carbonates, and 3) erroneous results if primary carbonate is transformed to a secondary carbonate.

Mineralogy by XRD is not able to identify and quantify amorphous carbonates, which results in underestimating the total CO_2 sequestration. For example, Turvey et al. (2018) documented hydrotalcite and hydrated Mg-carbonate minerals as carbon sinks in serpentinite mine wastes, yet, emphasized that the carbon sequestration rates were underestimated due to the inability to quantify non-crystalline phases by XRD.

Identifying and quantifying secondary carbonates is essential for using mineralogical approaches for carbon verification. However, distinguishing between primary and secondary phases can be difficult, particularly when the secondary mineral is also a primary mineral in the rock being used for CO_2 sequestration (Stubbs et al., 2022). For example, calcite is present in the Venetia kimberlite ore and is also a likely carbon sink as process waters are supersaturated with respect to this mineral. If new calcite formed; it would be nearly impossible to differentiate between the bedrock carbonate using solely XRD. Similarly, brucite and wollastonite skarn from this study contain pre-existing hydromagnesite and calcite, respectively. If the secondary carbonates were quantified without knowing the initial abundance, it would lead to erroneous carbon verification.

Mineralogical transformations during weathering may also confound carbon verification if not monitored closely. The formation of trona in experiments was misleading regarding CO_2 sequestration, given that there was no significant increase in TIC after 1 yr of weathering. Our interpretation is that trona mainly formed from the dissolution of primary calcite and release of Na from the kimberlite residues; thus, there was no net increase in TIC. Consequently, quantifying the increase in trona abundance without also quantifying calcite loss would lead to overestimating CO_2 sequestration. As another example, the dissolution of primary magnesite can lead to the formation of secondary hydromagnesite (e.g., Power et al., 2019), which, if quantified as a new carbon sink without accounting for the loss of magnesite, overestimates CO_2 sequestration.

4.3.2. Total inorganic carbon

Using TIC as a method for carbon verification is advantageous as it is an absolute measure of the stored CO_2 and accounts for amorphous phases unlike XRD (Table S2). However, TIC has two key limitations as a carbon verification method: 1) it fails to account for solubility trapping of CO_2 and 2) it is difficult to establish the initial TIC content in large complex systems (e.g., tailings impoundments).

In enhanced weathering studies, it is necessary to quantify solubility trapping of CO_2 as mineral trapping may not occur or be insignificant when pore waters are undersaturated with respect to carbonate minerals (Bach et al., 2019; Montserrat et al., 2017). Thus, TIC measurements of solid samples are inappropriate carbon verification method. For example, Stubbs et al. (2022) measured CO_2 fluxes of the same mineral feedstocks and kimberlite residues used in this study and observed a drawdown in CO_2 via solubility trapping in powdered kimberlite residues, and pulverized serpentinite and forsterite. As water evaporated CO_2 was degassed from the system unlike brucite and wollastonite skarn where there was a constant drawdown in CO_2 leading to mineral trapping.

Failure to accurately determine the initial baseline TIC content will lead to erroneous CO_2 sequestration estimations. Many rock types, including kimberlite, often have pre-existing carbonates that can be heterogeneously distributed through large rock formations, making the initial TIC content highly variable. Kimberlite residues sampled from Venetia have TIC contents ranging from 0.43 to 0.87% despite being collected within meters of each other. Extensive sampling (e.g., 1000s of samples) may be required to accurately determine the initial TIC content of a large open system such as an ERW site. In smaller systems with reactive minerals, such as the brucite and wollastonite skarn experiments, the increase in TIC was significantly greater than its variation amongst small masses, which can almost entirely be analyzed through replicate analyses.

4.3.3. Stable carbon and oxygen isotopes

Stable carbon and oxygen isotopes have been used to identify carbon sources and verify atmospheric CO_2 sequestration during weathering of

ultramafic mine wastes (Flude et al., 2017; Gras et al., 2017; Oskierski et al., 2013; Wilson et al., 2011). However, there are limitations to using stable isotopes for carbon verification, including 1) isotope signatures reflecting multiple carbon sources, 2) CO_2 exchange indicating atmospheric CO_2 sequestration, and 3) kinetic fractionation effects that obscure atmospheric CO_2 sequestration.

Secondary carbonates precipitating from mixed sources of CO_2 (e.g., atmospheric CO_2 and organic C) make it difficult to interpret stable isotope data. For example, Wilson et al. (2011) documented Ca-, Mg-, and Na-carbonate efflorescences within kimberlite mine wastes at the Diavik Diamond Mine that included powdery films at the surface, at depth, and thick crusts where processed sewage effluent had been deposited. Carbon fixed within these less common Na-carbonates has been either 1) a result of organic carbon mineralization (given that $F^{14}C > 1$) or 2) recycled from the dissolution of calcite in the kimberlite residues (Wilson et al., 2011) which is similar to what occurred in our kimberlite experiments (pathway 2D). Stable isotope data for Diavik consisted of either a mix of kimberlite and carbonate (Ca and/or Na-rich) or nesquehonite crusts that were relatively pure, i.e., no dilution from the kimberlite residues. The nesquehonite crusts were enriched in ^{13}C and ^{18}O, indicating atmospheric CO_2 sequestration, while Ca- and Na-carbonates had an organic carbon signal, suggesting the incorporation of carbon from waste organics (Wilson et al., 2011).

Failing to account for recycled or exchanged carbon will likely result in the overestimation of total carbon sequestered. During the precipitation of trona during kimberlite weathering experiments there was a decrease in TIC. It is likely that carbon was recycled between the primary and secondary carbonates and exchanged with atmospheric CO_2 rather than just the incorporation of new atmospheric carbon. CO_2 exchange between dissolved inorganic carbon and atmospheric CO_2 would increase $\delta\ ^{13}C$ and $\delta\ ^{18}O$ values, indicating atmospheric CO_2 incorporation as was observed in experiments (Fig. 6).

Despite clear indications of atmospheric CO_2 sequestration in brucite and wollastonite samples (TIC increases and secondary carbonate precipitation), $\delta^{13}C$ values were not indicative of atmospheric CO_2 incorporation as they decreased due to kinetic fractionation, which results when carbonate precipitation outpaces CO_2 supply (Power et al., 2013a; Wilson et al., 2010). Thus, kinetic fractionation may obscure atmospheric CO_2 sequestration. If solely relying on stable isotope data, it would suggest that weathering of brucite and wollastonite skarn did not result in atmospheric CO_2 sequestration. These findings suggest that stable isotope data should not be relied on as a sole method for carbon verification.

4.3.4. Radiocarbon

The incorporation of atmospheric CO_2 is reflected in the radiocarbon content of carbonate minerals. An advantage of ^{14}C analyses is that all modern carbon is accounted for regardless of its source, e.g., organic carbon and atmospheric CO_2. However, a fundamental limitation, similar to with stable carbon and oxygen isotopes, is that CO_2 exchange can be misleading. Finstad et al. (2023) performed ^{14}C analyses of carbonate samples collected from ultramafic rock surfaces to verify carbon storage. Results suggest that radiocarbon is a useful technique to verify and account for the proportion of atmospherically derived carbon; however, all potential carbon sources must be characterized and their ^{14}C signatures determined (e.g., host rocks, local atmospheric CO_2, surface and ground water). However, if primary carbonates were present in the ultramafic rocks at Dumont Nickel Project and Swift Creek Landslide (Finstad et al., 2023), it is possible that C exchanged and precipitated a new carbonate with a modern signal, confounding interpretations. For example, Gras et al. (2017) describe how the dissolution of bedrock carbonate occurs during weathering of Dumont residues and affects the stable carbon isotopes of the secondary carbonates; however, they suggest that calcite dissolution is a minor contributor. In the present study, brucite and wollastonite skarn experienced a clear incorporation of atmospheric CO_2 as the $F^{14}C$ increased, corresponding to substantial TIC increases. The $F^{14}C$ data of the kimberlite residues also showed substantial incorporation of modern carbon; however, there was no net gain in CO_2 based on TIC. As with the stable carbon isotope data, the ^{14}C data are misleading because the incorporation of modern carbon is due to CO_2 exchange with the atmosphere, not net sequestration of CO_2 from the atmosphere.

5. Conclusion

Two primary weathering reaction pathways were identified where there is either silicate/hydroxide dissolution leading to carbonate precipitation or dissolution and reprecipitation of carbonates. Four different techniques were used to help verify carbon storage which was consistent of 1) mineralogy, 2) total inorganic carbon, 3) stable carbon and oxygen isotopes, and 4) radiogenic isotopes. Laboratory wetting and drying experiments demonstrate that changes in TIC in kimberlite residues over time are variable, while stable isotopic compositions indicate atmospheric CO_2 is incorporated within secondary Na-carbonate phases without a net gain in CO_2, a less desirable pathway in the context of CO_2 sequestration. More reactive minerals including brucite and wollastonite skarn exhibited much greater increases in TIC and incorporation of modern carbon, despite a depletion in ^{13}C, indicating that CO_2 supply was rate-limiting for carbonation of these highly reactive minerals. Experimental samples were compared to yellow ground, a primary example of long-term weathering in a mining environment. This approach is exemplified by the conversion of blue ground to yellow ground that shows an approximate doubling of the TIC content with a clear presence of secondary carbonates as demonstrated by QEMSCAN. Both Voorspoed kimberlites were essentially radiocarbon dead; however, during weathering experiments, substantial modern carbon was incorporated into the kimberlite residues and brucite powder. Results demonstrate that in order to confirm storage of atmospheric CO_2, numerous analyses need to be compared to one another as part of the monitoring, reporting, and verification process.

Declaration of Competing Interest

The authors declare that they have no known competing financial and personal relationships that could influence the work produced in this manuscript.

Data availability

Data will be made available on request.

Acknowledgements

We are grateful for the funding provided by De Beers Group of Companies and support while at the Venetia Diamond Mine. We are thankful to Bob Vasily from Canadian Wollastonite skarn for providing material for the experiments. Funding was also provided by Natural Sciences and Engineering Research Council of Canada Discovery grants, a Natural Resources Canada Clean Growth grant, and a Mitacs Accelerate grant to Power and Wilson.

Appendix A. Supplementary data

Supplementary data to this article can be found online at https://doi.org/10.1016/j.chemgeo.2023.121674.

References

Acero, P., Ayora, C., Carrera, J., 2007. Coupled thermal, hydraulic and geochemical evolution of pyritic tailings in unsaturated column experiments. Geochim. Cosmochim. Acta 71 (22), 5325–5338.

Acero, P., Ayora, C., Carrera, J., Saaltink, M.W., Olivella, S., 2009. Multiphase flow and reactive transport model in vadose tailings. Appl. Geochem. 24 (7), 1238–1250.

Andrews, M.G., Taylor, L.L., 2019. Combating climate change through enhanced weathering of agricultural soils. Elements 15 (4), 253–258.
Arima, M., Kerrien, R., 1988. Jurassic kimberlites from Picton and Varty Lake, Ontario: geochemical and stable isotopic characteristics. Contrib. Mineral. Petrol. 99 (3), 385–391.
Bach, L.T., Gill, S.J., Rickaby, R.E.M., Gore, S., Renforth, P., 2019. CO_2 removal with enhanced weathering and ocean alkalinity enhancement: potential risks and co-benefits for marine pelagic ecosystems. Front. Clim. 1, 7.
Bea, S.A., et al., 2012. Reactive transport modeling of natural carbon sequestration in ultramafic mine tailings. Vadose Zone J. 11 (2).
Beerling, D.J., et al., 2018. Farming with crops and rocks to address global climate, food and soil security. Nat Plants 4 (3), 138–147.
Bish, D.L., Howard, S.A., 1988. Quantitative phase analysis using the Rietveld method. J. Appl. Crystallogr. 21, 86–91.
da Costa, A.J.M., 1989. Palmietfontein kimberlite pipe, South Africa—a case history. Geophysics 54, 689–700.
Daval, D., Martinez, I., Corvisier, J., Findling, N., Goffé, B., Guyot, F., 2009. Carbonation of Ca-bearing silicates, the case of wollastonite: Experimental investigations and kinetic modeling. Chem. Geol. 265, 63–78.
Daval, D., et al., 2010. The effect of silica coatings on the weathering rates of wollastonite (CaSiO3) and forsterite (Mg2SiO4): an apparent paradox?. In: Water Rock Interaction-WRI-13 Proc. 13th International Conference on Water Rock Interaction, pp. 713–717.
Declercq, J., Oelkers, E.H., 2014. CarbFix Report: PHREEQC Mineral Dissolution Kinetics Database.
Deines, P., Gold, D.P., 1973. The isotopic composition of carbonatite and kimberlite carbonates and their bearing on the isotopic composition of deep-seated carbon. Geochim. Cosmochim. Acta 37 (7), 1709–1733.
Deines, P., Langmuir, D., Harmon, R.S., 1974. Stable carbon isotope ratios and the existence of a gas phase in the evolution of carbonate ground waters. Geochim. Cosmochim. Acta 38 (7), 1147–1164.
EASAC, 2018. Negative Emission Technolgies: What Role in Meeting Paris Agreement Targets? German National Academy of Sciences Leopoldina.
Fall, M., Célestin, J.C., Han, F.S., 2009. Suitability of bentonite-paste tailings mixtures as engineering barrier material for mine waste containment facilities. Miner. Eng. 22 (9–10), 840–848.
Farquhar, G.D., Ehleringer, J.R., Hubick, K.T., 1989. Carbon isotope discrimination and photosynthesis. Annu. Rev. Plant Physiol. Plant Mol. Biol. 40, 503–537.
Farquhar, S.M., et al., 2015. A fresh approach to investigating CO_2 storage: experimental CO_2–water–rock interactions in a low-salinity reservoir system. Chem. Geol. 399, 98–122.
Fedortchouk, Y., Canil, D., 2004. Intensive variables in kimberlite magmas, Lac de Gras, Canada and implications for diamond survival. J. Petrol. 45 (9), 1725–1745.
Finstad, K.M., Smith, M.M., Beaudoin, G., Dipple, G., Aines, R.D., 2023. Radiocarbon analysis as a method for verifying atmospheric CO_2 uptake during carbon mineralization. Nucl. Inst. Methods Phys. Res. A 534, 35–38.
Flude, S., et al., 2017. The inherent tracer fingerprint of captured CO_2. Int. J. Greenh. Gas Control 65, 40–54.
Galimov, E.M., Ukhanov, A.V., 1989. The nature of the carbonate component of kimberlites. Geochem. Int. 337–348.
Giuliani, A., et al., 2014. Stable isotope (C, O, S) compositions of volatile-rich minerals in kimberlites: a review. Chem. Geol. 374-375, 61–83.
Gorski, C.A., Fantle, M.S., 2017. Stable mineral recrystallization in low temperature aqueous systems: a critical review. Geochim. Cosmochim. Acta 198, 439–465.
Gras, A., et al., 2017. Isotopic evidence of passive mineral carbonation in mine wastes from the Dumont Nickel project (Abitibi, Quebec). Int. J. Greenh. Gas Control 60, 10–23.
Haque, F., Santos, R.M., Dutta, A., Thimmanagari, M., Chiang, Y.W., 2019. Co-benefits of wollastonite weathering in agriculture: CO_2 sequestration and promoted plant growth. ACS Omega 4 (1), 1425–1433.
Harrison, A.L., Power, I.M., Dipple, G.M., 2013. Accelerated carbonation of brucite in mine tailings for carbon sequestration. Environ. Sci. Technol. 47 (1), 126–134.
Harrison, A.L., Dipple, G.M., Power, I.M., Mayer, K.U., 2015. Influence of surface passivation and water content on mineral reactions in unsaturated porous media: implications for brucite carbonation and CO_2 sequestration. Geochim. Cosmochim. Acta 148, 477–495.
Harrison, A.L., Benezeth, P., Schott, J., Oelkers, E.H., Mavromatis, V., 2021. Magnesium and carbon isotope fractionation during hydrated Mg-carbonate mineral phase transformations. Geochim. Cosmochim. Acta 293, 507–524.
Harrison, A.L., Schott, J., Oelkers, E.H., Maher, K., Mavromatis, V., 2022. Rates of carbon and oxygen isotope exchange between calcite and fluid at chemical equilibrium. Geochim. Cosmochim. Acta 335, 369–382.
Hill, R.J., Howard, C.J., 1987. Quantitative phase analysis from neutron powder diffraction data using the Rietveid method. J. Appl. Crystallogr. 20, 467–474.
Hua, Q., et al., 2022. Atmospheric radiocarbon for the period 1950–2019. Radiocarbon 64 (4), 723–745.
Huijgen, W.J.J., Witkamp, G.-J., Comans, R.N.J., 2006. Mechanisms of aqueous wollastonite carbonation as a possible CO_2 sequestration process. Chem. Eng. Sci. 61, 4242–4251.
Ignatov, P.A., et al., 2018. Zoning of faults and secondary mineralization of host rocks of kimberlites of the Maiskoe diamond deposit, Nakyn field, Yakutia. Geol. Ore Depos. 60 (3), 201–209.
IPCC, 2022. Climate Change 2022: Impacts, Adaptation and Vulnerability. Working Group II Contribution to the IPCC Sixth Assessment Report. Cambridge University Press.
Ito, M., 1986. Kimberlites and their ultramafic xenoliths from western Kenya. Tschermaks Mineral. Petrogr. Mitt. 35, 193–216.
Kamenetsky, V.S., Kamenetsky, M.B., Golovin, A.V., Sharygin, V.V., Maas, R., 2012. Ultrafresh salty kimberlite of the Udachnaya–East pipe (Yakutia, Russia): a petrological oddity or fortuitous discovery? Lithos 152, 173–186.
Kirkley, M.B., Smith, H.S., Gurney, J.J., 1989. Kimberlite carbonates - a carbon and oxygen stable isotope study. In: Kimberlites and Related Rocks, 1, pp. 264–281.
Kobelski, B.J., Gold, D.P., Deines, P., 1979. Variations in stable isotope compositions for carbon and oxygen in some South African and Lesothan kimberlites. In: Kimberlites, Diatremes and Diamonds: Their Geology, Petrology, and Geochemistry, 1, pp. 252–271.
Kojima, T., Nagamine, A., Ueno, N., Uemiya, S., 1997. Absorption and fixation and carbon dioxide by rock weathering. Energy Convers. Manag. 38, S461–S466.
Kuleshov, V.N., Ilupin, I.P., 1983. Carbon and oxygen isotope compositions for carbonates in Siberian kimberlite pipes. Int. Geol. Rev. 25 (11), 1352–1357.
Lee, X., et al., 2005. Carbon isotope of bulk organic matter: a proxy for precipitation in the arid and semiarid Central East Asia. Glob. Biogeochem. Cycles 19 (4) n/a-n/a.
Li, W., Beard, B.L., Li, C., Johnson, C.M., 2014. Magnesium isotope fractionation between brucite $Mg(OH)_2$ and Mg aqueous species: implications for silicate weathering and biogeochemical processes. Earth Planet. Sci. Lett. 394, 82–93.
Li, J., Hitch, M., Power, I.M., Pan, Y., 2018. Integrated mineral carbonation of ultramafic mine deposits-a review. Minerals 8 (4).
Lu, X., Carroll, K.J., Turvey, C.C., Dipple, G.M., 2022. Rate and capacity of cation release from ultramafic mine tailings for carbon capture and storage. Appl. Geochem. 140.
Mervine, E.M., et al., 2018. Potential for offsetting diamond mine carbon emissions through mineral carbonation of processed kimberlite: an assessment of De Beers mine sites in South Africa and Canada. Mineral. Petrol. 112, 755–765.
Montserrat, F., et al., 2017. Olivine dissolution in seawater: implications for CO_2 sequestration through enhanced weathering in coastal environments. Environ. Sci. Technol. 51 (7), 3960–3972.
Mook, W.G., Bommerson, J.C., Staverman, W.H., 1974. Carbon isotope fractionation between dissolved bicarbonate and gaseous carbon dioxide. Earth Planet. Sci. Lett. 22, 169–176.
Muhlinghuas, C., Scholz, D., Mangini, A., 2009. Modelling fractionation of stable isotopes in stalagmites. Geochim. Cosmochim. Acta 73 (24), 7275–7289.
O'Leary, M.H., 1981. Carbon isotope fractionation in plants. Phytochemistry 20 (4), 553–567.
Oskierski, H.C., Dlugogorski, B.Z., Jacobsen, G., 2013. Sequestration of atmospheric CO_2 in chrysotile mine tailings of the Woodsreef Asbestos Mine, Australia: quantitative mineralogy, isotopic fingerprinting and carbonation rates. Chem. Geol. 358, 156–169.
Oskierski, H.C., Dlugogorski, B.Z., Oliver, T.K., Jacobsen, G., 2016. Chemical and isotopic signatures of waters associated with the carbonation of ultramafic mine tailings, Woodsreef Asbestos Mine, Australia. Chem. Geol. 436, 11–23.
Paulo, C., et al., 2021. Evaluating feedstocks for carbon dioxide removal by enhanced rock weathering and CO_2 mineralization. Appl. Geochem. 129, 104955.
Peck, W.H., et al., 2023. Passive Carbon Sequestration Associated with Wollastonite Mining, Adirondack Mountains, New York. American Mineralogist.
Pokrovsky, O.S., Schott, J., 2004. Experimental study of brucite dissolution and precipitation in aqueous solutions: surface speciation and chemical affinity control. Geochim. Cosmochim. Acta 68 (1), 31–45.
Pokrovsky, O.S., Shirokova, L.S., Benezeth, P., Schott, J., Golubev, S.V., 2009. Effect of organic ligands and heterotrophic bacteria on wollastonite dissolution kinetics. Am. J. Sci. 309, 731–772.
Power, I.M., Harrison, A.L., Dipple, G.M., Southam, G., 2013a. Carbon sequestration via carbonic anhydrase facilitated magnesium carbonate precipitation. Int. J. Greenh. Gas Control 16, 145–155.
Power, I.M., et al., 2013b. Carbon mineralization: from natural analogues to engineered systems. Rev. Mineral. Geochem. 77 (1), 305–360.
Power, I.M., Harrison, A.L., Dipple, G.M., 2016. Accelerating mineral carbonation using carbonic anhydrase. Environ. Sci. Technol. 50 (5), 2610–2618.
Power, I.M., Kenward, P.A., Dipple, G.M., Raudsepp, M., 2017. Room temperature magnesite precipitation. Cryst. Growth Des. 17 (11), 5652–5659.
Power, I.M., et al., 2019. Magnesite formation in playa environments near Atlin, British Columbia, Canada. Geochim. Cosmochim. Acta 255, 1–24.
Power, I.M., Dipple, G.M., Bradshaw, P.M.D., Harrison, A.L., 2020. Prospects for CO_2 mineralization and enhanced weathering of ultramafic mine tailings from the Baptiste nickel deposit in British Columbia, Canada. Int. J. Greenh. Gas Control 94.
Power, I.M., et al., 2021. Carbonation, cementation, and stabilization of ultramafic mine tailings. Environ. Sci. Technol. 55 (14), 10056–10066.
Power, I.M., Wilson, S.A., Dipple, G.M., 2013c. Serpentinite carbonation for CO_2 sequestration. Elements 9 (2), 115–121.
Price, S.E., Russel, J.K., Kopylova, M.G., 2000. Primitive magma from the Jericho pipe, N.W.T., Canada: constraints on primary kimberlite melt chemistry. J. Petrol. 41 (6), 789–808.
Pronost, J., et al., 2012. CO_2-depleted warm air venting from chrysotile milling waste (Thetford Mines, Canada): Evidence for in-situ carbon capture from the atmosphere. Geology 40 (3), 275–278.
Renforth, P., 2012. The potential of enhanced weathering in the UK. Int. J. Greenh. Gas Control 10, 229–243.
Rietveld, H.M., 1969. A profile refinement method for nuclear and magnetic structures. J. Appl. Crystallogr. 2, 65–71.
Rollo, H.A., Jamieson, H.E., 2006. Interaction of diamond mine waste and surface water in the Canadian Arctic. Appl. Geochem. 21 (9), 1522–1538.
Sarma, B.S.P., Verma, B.K., 1996. Negative magnetisation contrast in Kimberlite search. Explor. Geophys. 27 (1), 21–24.

Sheppard, S.M.F., Dawson, J.B., 1975. Hydrogen, carbon and oxygen isotope studies of megacryst and matrix minerals from lesothan and South African kimberlites. Phys. Chem. Earth 9, 747–763.
Smith, R.S., Annan, A.P., Lemieux, J., Pedersen, R.N., 1996. Application of a modified GEOTEM® system to reconnaissance exploration for kimberlites in the Point Lake area, NWT, Canada. Geophysics 61 (1), 82–92.
Stamm, F.M., et al., 2019. The experimental determination of equilibrium Si isotope fractionation factors among H_4SiO_4 degrees, $H_3SiO_4^-$ and amorphous silica (SiO_2 center dot 0.32 H_2O) at 25 and 75 degrees C using the three-isotope method. Geochim. Cosmochim. Acta 255, 49–68.
Stubbs, A.R., et al., 2022. Direct measurement of CO_2 drawdown in mine wastes and rock powders: implications for enhanced rock weathering. Int. J. Greenh. Gas Control 113.
Tai, C.Y., Chen, W.R., Shih, S.-M., 2006. Factors affecting wollastonite carbonation under CO2 supercritical conditions. AICHE J. 52 (1), 292–299.
Tappe, S., et al., 2011. A fresh isotopic look at greenland kimberlites: cratonic mantle lithosphere imprint on deep source signal. Earth Planet. Sci. Lett. 305 (1–2), 235–248.
Taylor, L.L., et al., 2015. Enhanced weathering strategies for stabilizing climate and averting ocean acidification. Nat. Clim. Chang. 6 (4), 402–406.
Thom, J.G.M., Dipple, G.M., Power, I.M., Harrison, A.L., 2013. Chrysotile dissolution rates: implications for carbon sequestration. Appl. Geochem. 35, 244–254.
Turvey, C.C., et al., 2018. Hydrotalcites and hydrated Mg-carbonates as carbon sinks in serpentinite mineral wastes from the Woodsreef chrysotile mine, New South Wales, Australia: controls on carbonate mineralogy and efficiency of CO_2 air capture in mine tailings. Int. J. Greenh. Gas Control 79, 38–60.
USGS, 2020. Mineral Commodity Summaries - Wollastonite.
Ustinov, V.I., Ukhanov, A.V., Gavrilov, Y.Y., 1994. Oxygen isotope composition of the mineral assemblages in the stages of emplacement of kimbelites. Geochem. Int. 31 (8), 152–156.
Vanderzee, S.S.S., Dipple, G.M., Bradshaw, P.M.D., 2019. Targeting Highly Reactive Labile Magnesium in Ultramafic Tailings for Greenhouse-Gas Offsets and Potential Tailings Stabilization at the Baptiste Deposit, Central British Columbia (NTS 093K/13, 14). Geoscience BC.
Wagner, P.A., 1971. The Diamond Fields of Southern Africa: C. Struik (Pty) Ltd. (1st Impression, 1914).
Wilson, M.R., Kjarsgaard, B.A., Taylor, B., 2007. Stable isotope composition of magmatic and deuteric carbonate phases in hypabyssal kimberlite, Lac de Gras field, Northwest Territories, Canada. Chem. Geol. 242 (3–4), 435–454.
Wilson, S.A., et al., 2009a. Carbon dioxide fixation within mine wastes of ultramafic-hosted ore deposits: examples from the Clinton Creek and Cassiar chrysotile deposits, Canada. Econ. Geol. 104 (1), 95–112.
Wilson, S.A., Raudsepp, M., Dipple, G.M., 2009b. Quantifying carbon fixation in trace minerals from processed kimberlite: a comparative study of quantitative methods using X-ray powder diffraction data with applications to the Diavik Diamond Mine, Northwest Territories, Canada. Appl. Geochem. 24 (12), 2312–2331.
Wilson, S.A., Barker, S.L.L., Dipple, G.M., Atudorei, V., 2010. Isotopic disequilibrium during uptake of atmospheric CO_2 into mine process waters: implications for CO_2 sequestration. Environ. Sci. Technol. 44, 9522–9529.
Wilson, S.A., et al., 2011. Subarctic weathering of mineral wastes provides a sink for atmospheric CO_2. Environ. Sci. Technol. 45 (18), 7727–7736.
Wilson, S.A., et al., 2014. Offsetting of CO_2 emissions by air capture in mine tailings at the Mount Keith Nickel Mine, Western Australia: rates, controls and prospects for carbon neutral mining. Int. J. Greenh. Gas Control 25, 121–140.
Yang, Y., Lepech, M.D., Yang, E.-H., Li, V.C., 2009. Autogenous healing of engineered cementitious composites under wet–dry cycles. Cem. Concr. Res. 39 (5), 382–390.
Zeyen, N., et al., 2022. Cation exchange in smectites as a new approach to mineral carbonation.docx. Front. Clim. 4.